Title

The evolution of nonlinear subhorizon-scale entropy fluctuations in the early universe

Journal

The Astrophysical Journal, 423(1)

ISSN

0004-637X

Authors

Jedamzik, Karsten

Fuller, George M

Publication Date

1994-03-01

DOI

10.1086/173788

Peer reviewed

THE ASTROPHYSICAL JOURNAL, 423:33–49, 1994 March 1

THE EVOLUTION OF NONLINEAR SUBHORIZON-SCALE ENTROPY FLUCTUATIONS IN THE EARLY UNIVERSE

KARSTEN JEDAMZIK[1] AND GEORGE M. FULLER
Department of Physics, University of California, San Diego, La Jolla, CA 92093-0319
Received 1993 June 21; accepted 1993 August 30

ABSTRACT

We examine the damping of nonlinear subhorizon-scale entropy fluctuations in early epochs of the universe ($T \approx 100$ GeV to $T \approx 1$ keV) by neutrino-, baryon-, and photon-induced dissipative processes. Results of numerical evolution calculations are presented for broad ranges of initial fluctuation amplitudes and length scales. These calculations include a detailed treatment of neutrino inflation, neutron and proton diffusion, photon diffusive heat transport, and hydrodynamic expansion with photon-electron Thomson drag. Neutrino inflation is treated both in the diffusive heat transport regime where neutrinos are optically thick on the length scales of the fluctuations, and in the homogeneous heating regime where neutrinos are optically thin on these scales. We find considerable convergence in amplitude evolution for appreciable ranges in initial fluctuation length scales and amplitudes. Fluctuations produced with the right characteristics at very early times ($T \gtrsim 100$ GeV) are found to survive through the nucleosynthesis epoch.

Subject headings: early universe — hydrodynamics — radiative transfer

1. INTRODUCTION

The present model for the history of the early universe envisions significant departures from local thermal and chemical equilibrium associated with symmetry-breaking events. These events might include, for example, the quantum chromodynamics (QCD) epoch ($T \approx 100$ MeV), the electroweak transition ($T \approx 100$ GeV), and an inflationary epoch. Although the details and conclusions remain uncertain, such departures from thermal and chemical equilibrium at early epochs have been proposed as production sites for entropy fluctuations. By entropy fluctuations we mean any local deviations in the entropy per baryon from the cosmic average value. Entropy fluctuations could also result from processes associated with primordial black holes, cosmic strings, and domain walls. In this paper we wish to examine how an entropy fluctuation produced with a given amplitude and spatial dimension at a given epoch will subsequently evolve. We will not be concerned here with how fluctuations are produced, but rather with how their amplitudes and spatial scales change in time due to the expansion of the universe and neutrino, baryon, and photon dissipative processes.

The abundances of the elements emerging from the nucleosynthesis epoch can be sensitive to the existence of entropy fluctuations (cf. Mathews et al. 1990; Kurki-Suonio et al. 1988; Terasawa & Sato 1989a, b, c, 1990; Jedamzik, Fuller, & Mathews 1994; and the review of nonstandard big bang nucleosynthesis by Malaney & Mathews 1993). Observed light-element abundances can be used to constrain inhomogeneities at the nucleosynthesis epoch. It is hoped that these limits, in turn, may be used to constrain any processes in the very early universe which might generate entropy fluctuations. Successfully being able to constrain the physics of the early universe in the manner would depend on (1) knowing how fluctuations evolve from production at early epochs through the nucleosynthesis epoch and (2) knowing what the effects of such fluctuations on nucleosynthesis would be. This paper addresses the first of these issues.

The production of entropy fluctuations on subhorizon scales in the nonlinear regime (amplitude greater than unity) has been discussed extensively in the context of the QCD epoch (cf. Witten 1984; Applegate & Hogan 1985; Applegate, Hogan, & Scherrer 1987; Kajantie & Kurki-Suonio 1986; Kurki-Suonio 1988; Fuller, Mathews, & Alcock 1988; Applegate 1991; Malaney & Mathews 1993). There is no consensus on fluctuation characteristics to be expected from this epoch. In fact, recent lattice QCD results (cf. Brown et al. 1990) indicate that the chiral symmetry transition associated with this epoch leads to a second-order phase transition and, therefore, no phase separation and no fluctuation production. However, these results are not definitive, since they are dependent on lattice size and a proper treatment of dynamical quarks (Petersson 1991). Fluctuations associated with the QCD epoch might be generated by kaon condensate nuggets (Nelson 1990) through a mechanism which is independent of the order of the chiral symmetry phase transition.

The electroweak phase transition is expected to be weakly first order (Kirzhnits & Linde 1976). It has been proposed recently that baryogenesis may be associated with nonequilibrium processes proceeding on the surfaces of bubbles of the low-temperature phase in the cosmic electroweak transition (Shaposhnikov 1986, 1987, 1988; McLerran 1989; Cohen, Kaplan, & Nelson 1990, 1991a, b; Turok & Zadrozny 1990, 1991; Dine et al. 1991; McLerran et al. 1991). It may be that the entropy per baryon, and, hence, the baryon-to-photon ratio resulting from these baryogenesis scenarios, will be left with an inhomogeneous distribution across the horizon (Fuller et al. 1993). The generation of these entropy fluctuations might be related to the details of the nonequilibrium processes as well as the stochastic nature of bubble nucleation and coalescence.

Other events or processes in the early universe have been suggested as entropy fluctuation generators. For example, superconducting cosmic strings and associated large currents

[1] Present address: University of California, Lawrence Livermore National Laboratory, Livermore, CA 94550.

and magnetic fields could generate appreciable inhomogeneity in baryon density (Malaney & Butler 1989). It is conceivable that an inflationary epoch could generate nonlinear small-scale isocurvature fluctuations (Yokoyama & Suto 1991; Dolgov & Silk 1993). For a review of entropy fluctuation-generation mechanisms we refer the reader to Malaney & Mathews (1993).

Our goal in this paper is to describe the evolution in time of the amplitude, size, and shape of a nonlinear subhorizon-scale fluctuation with properties specified at some initial epoch. This problem has been discussed in previous work (Peebles 1965; Misner 1967; Hogan 1978; Heckler & Hogan 1993; Hogan 1993). Our calculations differ from those of previous studies in that we extend our survey to much higher temperatures ($T \approx 100$ GeV), we perform complete numerical multi–spatial-zone calculations including all relevant dissipative and hydrodynamic effects, we use a more sophisticated and detailed equation of state, and we employ the Boltzmann equation in our calculations of neutrino heat transfer. Our results, especially as regards the survivability of fluctuations produced at very early epochs, can differ from those of previous studies.

Fluctuations may be produced in the early universe with an adiabatic, isothermal, or isocurvature character (cf. Kolb & Turner 1990). It is conceivable that fluctuations could be produced which have aspects of all of these characteristics. Adiabatic fluctuations are not fluctuations in entropy per baryon, whereas isothermal or isocurvature fluctuations are entropy fluctuations. Once fluctuations enter the horizon, they evolve rapidly and nearly adiabatically to pressure equilibrium with the background environment (Hogan 1978). We will term any such fluctuation which has come to pressure equilibrium as an *isobaric* fluctuation.

In Figure 1 we present a schematic picture for entropy fluctuation classification and evolution. In this figure we show the ratio of entropy density in the fluctuation to average entropy density plotted against the ratio of baryon number density in the fluctuation to average baryon number density. All fluctuations evolve toward the isobaric line. Hydrodynamic evolution tracks toward pressure equilibrium for isothermal and isocurvature fluctuations are shown as dotted lines. Adiabatic fluctuations cease to exist when pressure equilibrium is attained. Once pressure equilibrium for nonadiabatic fluctuations is established, subsequent evolution proceeds largely along the isobaric line and is induced by neutrino, photon, and baryon dissipative processes.

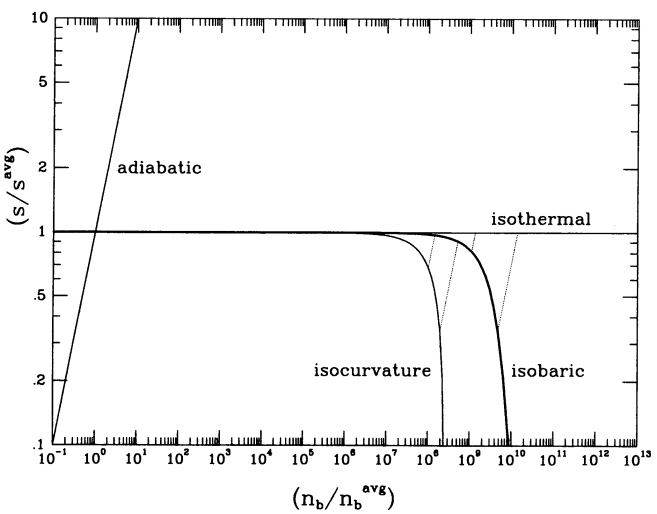

FIG. 1.—Schematic representation of the ratio of entropy density in fluctuations to the average entropy plotted against the ratio of the baryon number density in fluctuations to the average baryon number density. We show adiabatic, isothermal, isocurvature, and isobaric (*heavy line*) fluctuations. The dotted lines represent the tracks for the nearly adiabatic hydrodynamic expansion/contraction of fluctuations to pressure equilibrium.

In § 2 we consider the physics of neutrino, photon, and baryon dissipative processes. Section 3 presents numerical simulations for entropy fluctuation evolution. Conclusions are given in § 4.

2. DAMPING OF ISOBARIC ENTROPY FLUCTUATIONS

In this section we discuss the evolution of subhorizon-scale entropy fluctuations. A schematic representation of the kind of fluctuation we consider is shown in Figure 2. In this figure L^s is the mean separation between the centers of fluctuations, and L is the width of a square wave fluctuation. When fluctuations enter the horizon, they undergo rapid hydrodynamic expansion (or contraction) until they come into pressure equilibrium with their surroundings. Fluctuations which are initially purely adiabatic are completely erased by this process. Fluctuations which initially have an isocurvature or isothermal component are not erased by the expansion or contraction to pressure equilibrium. We will call fluctuations which have attained pressure equilibrium with their surroundings "isobaric fluctuations." In this paper we will consider the subsequent damping of isobaric fluctuations by neutrino, baryon, and photon dissipative processes.

We define the baryon number overdensity distribution, $\Delta(x)$, by

$$n_b(x) = \bar{n}_b(1 + \Delta(x)) , \tag{1a}$$

where $n_b(x)$ is the proper net baryon number density at space coordinate x, and $\bar{n}_b$ is the average proper net baryon number density (see Fig. 2). We take the average proper number density at an epoch with scale factor R to be

$$\bar{n}_b(x) = \bar{N}_b(x)\left(\frac{R_{100}}{R}\right)^3 , \tag{1b}$$

where $\bar{N}_b(x)$ is the average proper number density at $T = 100$ MeV, and we take $R = R_{100}$ when $T = 100$ MeV. In what follows we choose $R_{100} = 1$.

The distribution of energy density in relativistic particles, $\varepsilon_{rel}(x)$, is defined in terms of the horizon average of this quan-

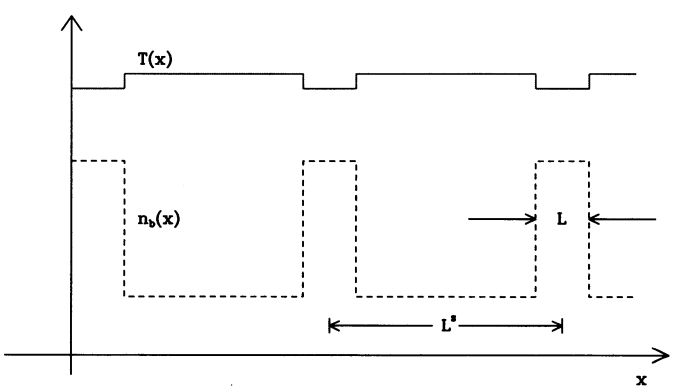

FIG. 2.—Three square wave fluctuations are shown. The net baryon number density $n_b(x)$ and the plasma temperature $T(x)$ are shown as functions of length scale x. The size of the high-density region of a fluctuation, or fluctuation length scale, is L, and the mean separation between centers of fluctuations is L^s.

tity, $\bar{\varepsilon}_{\rm rel}$, by

$$\varepsilon_{\rm rel}(x) = \bar{\varepsilon}_{\rm rel}(1 + 4\delta(x)) \, . \tag{2}$$

In this expression $4\delta(x)$ is then the deviation of the energy density from its average value at position x. We will be concerned with times early enough that the cosmic energy density is dominated by highly relativistic particles. The average energy density in relativistic particles in the dilute high-entropy conditions of the early universe is

$$\bar{\varepsilon}_{\rm rel} = g_{\rm eff}(\bar{T}) a \bar{T}^4 \, , \tag{3}$$

where $a = \pi^2/30$, $\bar{T}$ is the cosmic average temperature, and $g_{\rm eff} = \sum_b g_b + \frac{7}{8} \sum_f g_f$ is the number of degrees of freedom in relativistic bosons (b) and fermions (f). In this sum we will count only those particles with mean free path l smaller than the spatial dimension of the fluctuation. This typical spatial dimension, or fluctuation length, we denote as L (see Fig. 2).

In the limit where $\delta(x) \ll 1$ and in epochs where $g_{\rm eff}$ can be approximated as constant in time, we find that

$$\delta(x) \approx \frac{T(x) - \bar{T}}{\bar{T}} \, , \tag{4}$$

so that in this limit $\delta(x)$ is just the deviation from the cosmic average temperature at coordinate x.

We can get a rough idea of how fluctuations come into pressure equilibrium with their surroundings if we assume that baryons contribute perfect gas pressure $P_b = n_b T$ and relativistic particles contribute pressure $P_{\rm rel} = \frac{1}{3}\varepsilon_{\rm rel}$. In the following sections we will check the validity of these assumptions, and we will find significant deviation from perfect gas pressure at high temperatures $T \gtrsim 30$ MeV. Nevertheless, with these assumptions the demand for pressure equilibrium between the interior and exterior of a fluctuation implies

$$\tfrac{1}{3}\bar{\varepsilon}_{\rm rel}(1 + 4\delta(x)) + \bar{n}_b(1 + \Delta(x))\bar{T}(1 + \delta(x)) \approx \tfrac{1}{3}\bar{\varepsilon}_{\rm rel} + \bar{n}_b\bar{T} \, . \tag{5}$$

In the limit where $\delta \ll 1$ this expression reduces to

$$\delta(x) = -\frac{1}{4}\left(\frac{\bar{n}_b\bar{T}}{(1/3)\bar{\varepsilon}_{\rm rel}}\right)\Delta(x) \approx -\frac{1}{4}\left(\frac{\bar{P}_b}{\bar{P}_{\rm rel}}\right)\Delta(x) \approx -\frac{\Delta(x)}{\bar{s}} \, , \tag{6}$$

with $\bar{s}$ the average entropy per baryon in the early universe. Hereafter, a bar over any quantity denotes the average value of that quantity over the whole horizon volume unless indicated otherwise.

In the early universe the average entropy per baryon is a large quantity,

$$\bar{s} \approx 2.6 \times 10^8 \Omega_b^{-1} h^{-2} \, . \tag{7}$$

Here Ω_b is the fraction of the closure density contributed by baryons, and h is the Hubble constant in units of 100 km s^{-1} Mpc^{-1}. The average entropy per baryon $\bar{s}$ is constant with time in the limit where we can neglect baryon number violating processes ($T \lesssim 100$ GeV), black hole production and evaporation, and dissipative processes. Note that $\bar{s}$ is large enough that fluctuations will have $\delta < 1$ for $\Delta \lesssim 10^9$.

Pressure equilibrium for fluctuations is obtained initially by hydrodynamic expansion. The expansion of an entropy fluctuation can be rapid enough that we can regard it as a nearly adiabatic process. After pressure equilibrium is established, we expect the temperature in the fluctuation to be lower than $\bar{T}$ (see Fig. 2). Subsequent heat and entropy flow into the fluctuation will tend to cause the fluctuation to expand to a new pressure equilibrium. Entropy will flow into the fluctuation until the average entropy per baryon in the fluctuation matches the background average. Heat flow, or other dissipative processes, will of course generate entropy. In practice, however, the entropy generation due to dissipative processes is negligible for fluctuations with initial $\delta \ll 1$. The fluctuation will evolve through a succession of pressure equilibrium states if the heat transport time is long compared with a hydrodynamic expansion time.

The approximate timescale to attain pressure equilibrium between the fluctuation and the environment is the sound travel time, τ_p, over the fluctuation length L. The timescale to transform an initially isobaric fluctuation into an isothermal fluctuation is a typical heat transport timescale τ_h. The ratio of the hydrodynamic expansion time scale (or sound crossing time) to the typical heat transport time is

$$\frac{\tau_p}{\tau_h} \sim \frac{L/v_s}{L^2/D_h} \sim \frac{g_t}{g_{\rm eff}}\frac{l}{L} \, , \tag{8a}$$

where $v_s \approx c/\sqrt{3}$ is the speed of sound for a relativistic fluid. The heat diffusion constant is roughly $D_h \sim c(g_t/g_{\rm eff})l$, where l is a typical mean free path for heat-transporting particles, and g_t is the number of degrees of freedom which are effective in heat transport. Equation (8a) is only valid in the diffusive limit for heat transport, where $l < L$.

Particles with $l > L$ are free-streaming on the scale of the fluctuation. Even in this limit particles can still transport heat into the fluctuation. For neutrinos with $l > L$ we find a heating rate $\tau_h^{-1} \sim (g_t/g_{\rm eff})c/l$, which yields

$$\frac{\tau_p}{\tau_h} \sim \frac{g_t}{g_{\rm eff}}\frac{L}{l} \, . \tag{8b}$$

We conclude that the assumption that fluctuations evolve through a succession of pressure equilibrium configurations is valid in the extreme diffusive ($l \ll L$) and "homogeneous" ($l \gg L$) heating limits. Borrowing terminology from radiation transport studies, we can describe these limits as "optically thick" and "optically thin," respectively.

For an intermediate mean free path, $l \sim L$, the heating and pressure equilibrium timescales become comparable, and the calculation of the damping of fluctuations by heat flow would require a detailed solution of the Boltzmann equation. However, in the case of neutrino heat transport in the early universe we expect the approximation of pressure equilibrium to hold fairly well, since neutrinos go quickly from optically thick to optically thin on the scale of the fluctuation. Furthermore, the ratio $g_t/g_{\rm eff}$ is a small quantity for neutrino heat transport in the early universe, which tends to make the ratio in equations (8a) and (8b) small.

Baryon number fluctuations which are formed on subhorizon scales in epochs with $T > 50$ MeV have negligible self-gravity. However, self-gravity can be important for superhorizon-scale fluctuations. A rough estimate for the ratio of pressure forces F_p to gravitational forces F_g on the edge of a square wave fluctuation gives

$$\frac{F_p}{F_g} \sim 10^{16}\Delta^{-1}(\Omega_b h^2)^{-1}\left(\frac{L_{100}}{m}\right)^{-2} \, , \tag{9}$$

where L_{100} is the fluctuation length L measured on a "comoving" scale at an epoch of $T = 100$ MeV in a manner to be described below.

We will frequently refer proper lengths to a "comoving" scale at $T = 100$ MeV. The fluctuation length L and the

separation length L^s between adjacent fluctuations as measured on the $T = 100$ MeV scale are denoted by L_{100} and L^s_{100}, respectively. At an epoch where the temperature is T and the scale factor is $R(T)$, the relation between a proper length L and the associated "comoving" length L_{100} is

$$L = L_{100}\left[\frac{R(T)}{R_{100}}\right]. \quad (10)$$

If the product RT were constant with time, then we could write $R(T)/R_{100} = (100\ \text{MeV})/T$. However, particle annihilation epochs change the value of RT (e.g., $e^{\pm}$ annihilation; $\mu^{\pm}$ annihilation; quark annihilation or QCD transition). Figure 3 shows $R(T)(T/100\ \text{MeV})$ for $10^{-3}\ \text{MeV} < T < 100\ \text{MeV}$, including a numerical treatment of all relevant annihilation epochs. In this figure we assume that the quark-hadron transition occurs at higher temperatures, and we ignore pion degrees of freedom.

2.1. *Neutrino Inflation*

The neutrino mean free path l_ν is a rapidly varying function of temperature in the early universe,

$$l_\nu = \beta G_F^{-2} T^{-5} \approx 8 \times 10^{-6} m \left(\frac{T}{\text{GeV}}\right)^{-5} (N_l + 3N_q)^{-1}, \quad (11)$$

where G_F is the Fermi constant and N_l is the number of relativistic weakly interacting leptons at temperature T. These will include $e^{\pm}$, $\mu^{\pm}$, $\tau^{\pm}$, ν_e, $\bar{\nu}_e$, ν_μ, $\bar{\nu}_\mu$, ν_τ, $\bar{\nu}_\tau$, whenever their masses satisfy $m_l < T$. Similarly, N_q is the number of relativistic quark flavors at temperature T and may include u, d, s, c, b, and t. For example, at a temperature below that for quark annihilation $N_l \approx 10$ ($e^{\pm}$, $\mu^{\pm}$, and six neutrino species) and $N_q = 0$. Here we have neglected neutrino-pion scattering. The dimensionless quantity β depends on neutrino flavor, the types of relativistic leptons (quarks) in equilibrium at temperature T, and the exact lepton (quark) weak couplings. Heckler & Hogan (1993) have considered neutrino scattering in a weakly coupled relativistic plasma at zero chemical potential. They found that plasma screening corrections are negligible, so that neutrinos can be approximated as scattering incoherently off single particles.

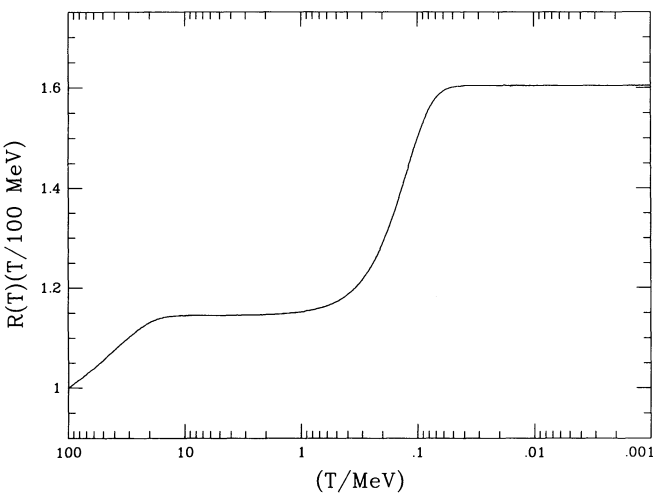

FIG. 3.—Product of cosmic scale factor and temperature, $R(T)(T/100$ MeV), plotted against temperature T in MeV. We take $R = 1$ at $T = 100$ MeV.

Neutrinos are very efficient heat transporters at any time in the early universe between the epochs of the electroweak phase transition ($T \approx 100$ GeV) and neutrino decoupling ($T \approx 1$ MeV). Before the electroweak phase transition, neutrino heat transport is inefficient, since for vanishing weak-gauge boson masses ($M_{Z,W} = 0$) the neutrino mean free path becomes small. Since the neutrino mean free path changes considerably over the history of the universe, where we follow entropy fluctuations, we will have to treat neutrino heat transport in two different limits: the homogeneous limit, $l_\nu > L$, and the diffusive limit, $l_\nu < L$.

In the homogeneous limit neutrinos are free-streaming through the fluctuation, so that neutrinos are optically thin on the scale of the fluctuation L. This implies that the neutrino energy density is homogeneous on these scales with $\varepsilon_\nu(x) = \bar{\varepsilon}_\nu$. In other words, the temperature for neutrinos is now slightly larger than the temperature for other relativistic particles inside the fluctuation. In this case neutrino scattering will tend to transfer energy into the fluctuation. The heat deposition rate in a fluctuation of size L is equal to the number of scattering events per unit time multiplied by the average energy transfer per collision. The scattering event rate is the neutrino flux $[\sim(g_\nu/10)T^3]$ times the weak cross section ($\sim G_F^2 T^2$) times the total number of targets within the fluctuation $[\sim(7/8)(2/10)(N_l + 3N_q)T^3L^3]$, assuming natural units $c = \hbar = 1$.

The fractional difference in temperature between the neutrinos and the rest of the particles in the fluctuation at position x is just $\delta(x)$. The average energy transfer per collision at position x is then roughly $\delta(x)T_\nu$, where T_ν is the homogeneous neutrino distribution temperature. Note that $T_\nu = \bar{T}$. These arguments yield the rate of change of energy density in the fluctuation,

$$\frac{\partial \varepsilon(x)}{\partial t} \approx -F G_F^2 \delta(x) \bar{T}^9, \quad (12)$$

where F is a numerical factor. At temperature $T \lesssim 50$ MeV we can approximate $F \approx (g_e g_\nu/100) \approx 0.2$, where $g_e = (\frac{7}{8})2N_e$, $N_e = 2$, and $g_\nu = (\frac{7}{8})6$. This naive estimate for the homogeneous neutrino heating rate turns out to be low compared with that derived from our detailed numerical treatment.

We have computed the homogeneous neutrino heating rate by using the Boltzmann transport equation. Specifically, we evaluated the collision integral term in the Boltzmann equation. In this calculation we solved for the energy transfer between a relativistic neutrino Fermi-Dirac distribution at temperature $\bar{T}$ and a relativistic Fermi-Dirac $e^{\pm}$ distribution at a lower temperature $\bar{T}(1 - \delta)$. The calculation neglects Fermi blocking effects on scattering particles, which is a fair approximation in the early universe, resulting in small errors which will not alter our conclusions. Our numerical result has the same form as equation (12) but has $F = 1.869$, so that the net heating rate is nearly an order of magnitude larger than the simple estimate. This result is not surprising, however, since the naive estimate of equation (12) does not take account of the contribution to heating from annihilation processes such as $e^+e^- \leftrightarrow \nu\bar{\nu}$. We include these processes in our numerical calculation. These processes dominate the energy deposition, accounting for 70% of F.

In the limit where $l_\nu > L$ we can employ equations (2) and (3) to rewrite equation (12) as

$$\frac{d\delta(x)}{dt} \approx -F^* \frac{g_\nu}{g_{\text{eff}}} \frac{1}{l_\nu} \delta(x), \quad (13a)$$

where

$$F^* = \frac{\beta}{g_\nu}\frac{1}{4a}F\,. \tag{13b}$$

Note that F^* is roughly independent of g_ν, N_l, and N_q.

When $l_\nu < L$, the optically thick limit obtains and we can approximate the neutrino heating as arising from neutrino diffusion. In this limit we can express the time evolution of $\delta(x)$ for a spherical fluctuation as

$$\frac{\partial\delta(r_{100})}{\partial t} = \frac{D_h}{R^2}\frac{1}{r_{100}^2}\frac{\partial}{\partial r_{100}}\left[r_{100}^2\frac{\partial\delta(r_{100})}{\partial r_{100}}\right], \tag{14}$$

where r_{100} is the radial coordinate of a spherical fluctuation measured on our comoving scale at $T = 100$ MeV, and $D_h \sim (g_\nu/g_{\rm eff})l_\nu$ is the heat diffusion constant. For a two-zone square wave fluctuation in the limit where $l_\nu < L$ we find

$$\frac{d\delta}{dt} = -\lambda^*\frac{g_\nu}{g_{\rm eff}}\frac{l_\nu}{L^2}\delta\,, \tag{15}$$

with λ^* a numerical factor of order unity. In this two-zone approximation for the density and temperature distribution of a spherical fluctuation, 4δ represents the fractional energy density difference between the inside (zone 1) and the outside (zone 2) of the fluctuation. Matching the heating rates in the diffusive and homogeneous limits for $l_\nu = L$, we obtain $\lambda^* = F^*$.

We now consider a two-zone square wave fluctuation, which will serve to illustrate the typical damping histories for fluctuations. A simple prescription for calculating the damping of isobaric square wave baryon number fluctuations by neutrino heat transport is as follows. If in time t a fluctuation is heated by $d\delta$, it has to expand adiabatically by $dL_{100} = L_{100}\,d\delta$ in order to reestablish pressure equilibrium. Thus,

$$\frac{1}{L_{100}}\frac{dL_{100}}{dt} = \frac{d\delta}{dt}\,, \tag{16}$$

where $L_{100} = L/R$ as before. Baryon number within the fluctuation is conserved during the adiabatic expansion of the fluctuation, and so the quantity $(1+\Delta)L_{100}^3$ is time-independent. In order to obtain the rate of increase in radius (or "inflation" rate) of isobaric square wave baryon number fluctuations, we integrate equation (16), using equation (13) in the homogeneous limit, and equation (15) in the diffusive limit. To accomplish this, we need to know the temperature difference δ as a function of the baryon number overdensity Δ for a fluctuation in pressure equilibrium.

The pressure due to relativistic particles can be written

$$P_{\rm ref} = f_p\,\varepsilon_{\rm rel}\,, \tag{17}$$

with $f_p = \frac{1}{3}$, except during epochs of lepton or quark annihilations. Figure 4 shows $f_p(T)$ during the e^+e^- annihilation. The value of f_p drops from $f_p = \frac{1}{3}$ to $f_p = 0.28$ at $T \approx 0.2$ MeV. At this temperature a major fraction of the kinetic energy of the relativistic gas is converted to rest mass energy of e^+e^- pairs. This rest mass makes zero contribution to the pressure.

We consider four temperature regimes in which there are natural limits for the pressure contributed by baryons. At temperatures below the QCD transition, baryon number is carried by color singlet baryonic states. In the regime after the QCD transition the kinematics of baryons can be taken to be approximately nonrelativistic. Below $T \approx 30$ MeV, baryons

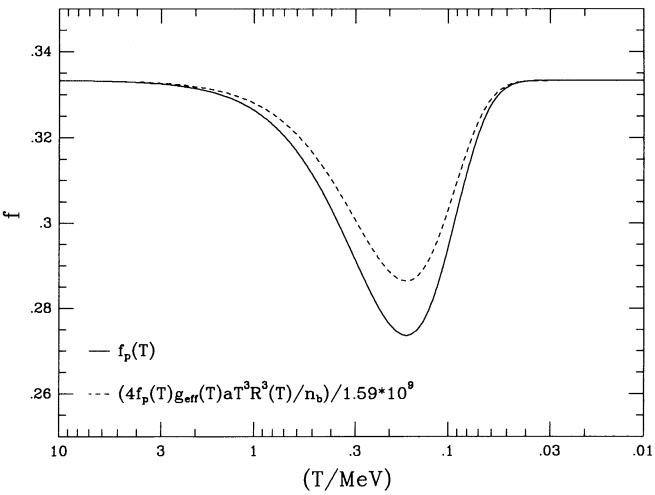

FIG. 4.—Proportionality constant f_p (*solid line*) between pressure exerted by relativistic particles and the energy density in relativistic particles plotted against temperature T in MeV. Also shown is the temperature dependence of the proportionality constant between deviation in relativistic energy density and the baryon overdensity within a fluctuation (*dashed line*).

exert perfect gas pressure P_b,

$$P_b = n_b T \approx \bar{n}_b\bar{T}(1+\Delta)\,. \tag{18}$$

The pressure contribution of the excess electrons needed for charge neutrality is negligible compared with the baryon pressure. The entropy per baryon is so high that the net number of electrons is small compared with the number of electron-positron pairs. Requiring pressure equilibrium as we did in equation (6), we obtain, for $T \lesssim 30$ MeV,

$$\delta \approx -\frac{1}{4}\left(\frac{\bar{n}_b T}{f_p\,\bar{\varepsilon}_{\rm rel}}\right)\Delta\,. \tag{19}$$

In Figure 4 we show the proportionality constant between Δ and δ through the e^+e^- annihilation epoch. In order to keep the fluctuation in pressure equilibrium during the e^+e^- annihilation process, δ has to increase. An increase in δ enhances heat flow into the fluctuation. During the e^+e^- annihilation at $T \sim 0.5$–0.05 MeV there are no particles which are efficient heat transporters, so that the pair-annihilation effect is unimportant. However, during epochs of quark annihilation at high temperatures or muon and pion annihilation at $T \sim 100$ MeV, the neutrino is an efficient heat transporter, and heat transport efficiency is slightly enhanced during the annihilation epochs.

Thermally produced baryon-antibaryon pairs are still abundant enough for $T \gtrsim 30$ MeV to modify the pressure from the perfect gas limit in equation (18). We find

$$P_b \approx T(n_{\rm pair}^2 + n_b^2)^{1/2}\,, \tag{20}$$

where

$$n_{\rm pair} \approx \left(\frac{2}{\pi}\right)^{3/2}(mT)^{3/2}\exp\left(-\frac{m}{T}\right)\left(1+\frac{15}{8}\frac{T}{m}\right) \tag{21}$$

is the total proton (neutron) plus antiproton (antineutron) particle density of a zero chemical potential Fermi gas at temperature T. The baryon mass is taken to be m. The overpressure exerted by the net baryon number falls below perfect gas pressure, since increasing the baryon number of a $\mu_b = 0$ Fermi gas by 2 is equivalent to adding one baryon and annihilating one antibaryon. For a temperature approaching the

Hagedorn temperature $T_H \sim 140$ MeV (Hagedorn 1971), the actual baryonic particle density exceeds the expression for n_{pair} in equation (21) due to the existence of thermally produced baryonic resonances. Since baryon number can be carried by additional degrees of freedom, the resulting overpressure due to extra net baryon number is further decreased for $T \to T_H$ (Alcock, Fuller, & Mathews 1987). Note that equation (20) reduces to the perfect gas pressure limit of equation (18) when $n_{pair} \ll n_b$.

We can estimate a temperature difference δ between the inside of a fluctuation and the cosmic background environment from pressure equilibrium,

$$\delta = -\frac{1}{4}\frac{\bar{T}}{f_p \bar{\varepsilon}_{rel}}\{[n_{pair}^2 + \bar{n}_b^2(1+\Delta)^2]^{1/2} - (n_{pair}^2 + \bar{n}_b^2)^{1/2}\} . \quad (22)$$

In Figure 5 we illustrate the decrease of fluctuation temperature difference δ at high temperatures for three different fluctuation overdensities Δ. The results shown in this figure do not include baryonic resonances. We show the ratio δ/δ_{pg}, with δ_{pg} the temperature difference derived using perfect gas pressure for baryons but with no baryon-antibaryon pairs. It is interesting to note that at high temperatures, but after the QCD transition, fluctuations with net baryon number ($\mu_b \neq 0$) can *almost* coexist in thermodynamic equilibrium with a vanishing chemical potential ($\mu_b = 0$) phase.

For times earlier than the QCD transition baryon number is carried by relativistic quarks. The QCD equation of state in the strong QCD coupling limit ($\alpha_s \sim 1$) is uncertain. The strong coupling limit obtains for $T \lesssim 3$–5 GeV (Mueller 1985). In the weak QCD coupling limit ($\alpha_s \ll 1$) we can approximate the equation of state as that of a relativistic ideal Fermi gas with net baryon number density n_b and small baryon chemical potential $\mu_b \ll T$,

$$P_q = \frac{7}{4} N_q a T^4 + 9 N_q^{-1}\frac{n_b^2}{T^2} , \quad (23)$$

where N_q is the number of relativistic quark flavors, and P_q is the total pressure of quark-antiquark pairs plus net baryon number. The overpressure due to net baryon number is the second term in equation (23). First-order perturbative strong interaction corrections would increase this term by a factor $(1 - 2\alpha_s/\pi)^{-1}$ (Mueller 1985). Using equation (23), we obtain for the temperature difference between the interior and exterior of a two-zone fluctuation

$$\delta = -\frac{9}{4 f_p \bar{\varepsilon}_{rel}}\frac{\bar{n}_b^2}{\bar{T}^2}\frac{1}{N_q}[(\Delta+1)^2 - 1] . \quad (24)$$

We are now in a position to integrate equation (16) and find by how much a fluctuation inflates. We take $F^* = 0.747$ and $\beta = 2.762$, and we assume that these quantities are approximately temperature-independent. The QCD transition is taken to be at $T = 100$ MeV, and the electroweak phase transition is taken to occur at a temperature above $T = 100$ GeV. Our estimate treats all quark and lepton annihilations as occurring instantaneously at temperature $T = m$. Quark masses are taken here to be $m_u = m_d = 0$, $m_s = 100$ MeV, $m_c = 1.35$ GeV, $m_b = 5$ GeV, and $m_t > 100$ GeV. We take the muon mass as $m_\mu = 105.7$ MeV and the τ lepton mass as $m_\tau = 1.78$ GeV. We take account of the increase of scale factor times temperature (RT) and decrease of statistical weight, g, during the annihilation epochs. The scale factor R depends on temperature as

$$R = \left(\frac{g_s}{10.75}\right)^{-1/3}\left(\frac{T}{100\ \text{MeV}}\right)^{-1} , \quad (25)$$

assuming complete pion and muon annihilation at $T = 100$ MeV ($g_s = 10.75$). The time-temperature relationship is

$$t = (2.42\ \text{s}) g^{-1/2}\left(\frac{T}{\text{MeV}}\right)^{-2} , \quad (26)$$

for a simple radiation-dominated expansion. For the early universe we calculate an average net baryon number density,

$$\bar{n}_b = 1.7 \times 10^{-9} g_s \Omega_b h^2 \bar{T}^3 . \quad (27)$$

In equation (26) we define the total statistical weight in relativistic particles to be $g = \sum_b g_b (T_b/T)^4 + (\frac{7}{8})\sum_f g_f (T_f/T)^4$, where we recognize that decoupled particles may have temperatures (T_b, T_f) which differ from the plasma temperature (T). The relevant statistical weight for entropy density, g_s, enters into equations (25) and (27) and is defined as $g_s = \sum_b g_b (T_b/T)^3 + (\frac{7}{8})\sum_f g_f (T_f/T)^3$.

We have done numerical calculations for two-zone square wave fluctuations based on the above approximations. We have also generalized this calculation to include many zones of different $n_b(x)$ and have thus obtained a better approximation to the continuum limit. We will first discuss our results for two zones and then will present our results for the multizone calculation in § 3.

In Figure 6 we show the evolution of neutrino mean free path $l_\nu^{100} = l_\nu/R$ and fluctuation length $L_{100} = L/R$ for three different overdensities, assuming an initial fluctuation length $L_{100}^i = 10^{-8}$ m. The proper fluctuation length of very high amplitude fluctuations increases at almost the same rate as the neutrino mean free path until the overdensity Δ is reduced by several orders of magnitude and the neutrinos become optically thin on the scale of the fluctuation. Therefore, most of the damping of nonlinear entropy fluctuations occurs in the diffusive limit ($l_\nu < L$). Note that the neutrino mean free path increase, dl_ν/dt, approaches the speed of light near neutrino

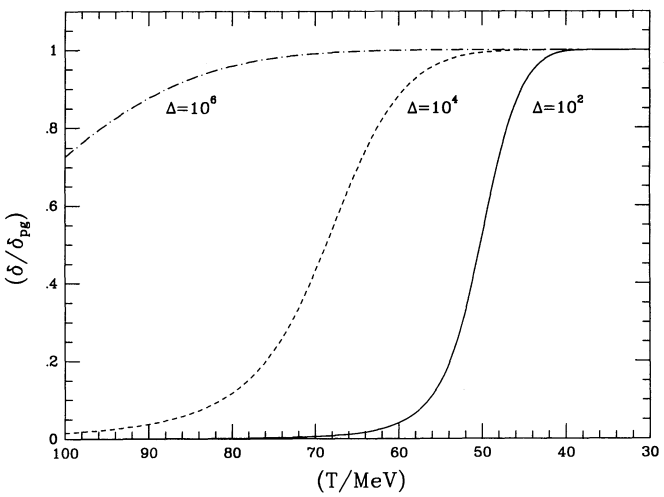

FIG. 5.—Plot of the ratio of the temperature (or energy density) deviations in a fluctuation for two different baryon equations of state against temperature. Here δ_{pg} is the deviation using a perfect gas Maxwell-Boltzmann equation of state for neutrons and protons, while δ is the deviation including baryon-antibaryon pairs. We show this ratio for three baryon overdensities Δ.

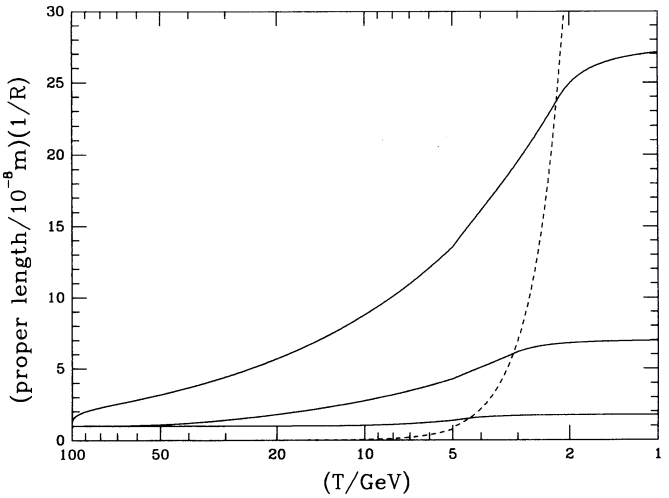

FIG. 6.—Proper radius in units of 10^{-8} m multiplied by R^{-1}, shown as a function of temperature for three different initial fluctuation amplitudes. In all three fluctuations an initial radius $L_{100} = 10^{-8}$ m is assumed. The fluctuations are distinguished by different initial baryon-to-entropy ratios $(n_b/s)_i = 10^{-1}$, 10^{-3}, and 10^{-5}. The neutrino mean free path l_ν^{100} is also displayed (*dashed line*).

decoupling ($T \approx 1$ MeV). The neutrino mean free path and the fluctuation length appear slightly discontinuous at $T = 5$ GeV because of our oversimplified treatment of $b\bar{b}$ annihilation. However, the discontinuities are small because of the large number of degrees of freedom at this epoch in the early universe. The results of an exact treatment of annihilation for a single degree of freedom would not differ appreciably from our estimates.

Figure 7 shows the results of our two-zone calculation for the damping of fluctuations by neutrino inflation between $T = 100$ GeV and $T = 100$ MeV. We display the final baryon-to-entropy ratio $(n_b/s)_f$ of inflated fluctuations as a function of initial fluctuation length L^i_{100} for five different initial baryon-to-entropy ratios $(n_b/s)_i$. We find considerable convergence in $(n_b/s)_f$ for a broad range of initial amplitudes $(n_b/s)_i$, when fluctuations have small initial length scales. Fluctuations with very small length scales $L^i_{100} \lesssim 10^{-14}$ m will be damped to a characteristic $(n_b/s)_f \approx 2 \times 10^{-8}$. Fluctuations with large initial length scales show little damping from neutrino inflation. Neutrino inflation becomes an important damping process for fluctuations with initial length scales smaller than some critical length. This critical length decreases as the initial fluctuation amplitude decreases. In Figure 7 the electroweak epoch horizon scale ($T = 100$ GeV) is approximately at the far right-hand end of the horizontal axis. Large overdensity fluctuations with large initial length scales have significant damping from neutrinos during the strong QCD coupling epoch. The uncertainties in the equation of state at this epoch translate into uncertainties in our damping estimates. We show our results as dashed lines in this uncertain damping regime.

In Figure 8 we display our results for neutrino inflation of fluctuations between $T = 100$ MeV and $T = 1$ MeV. In this calculation we have neglected the effects of baryonic and mesonic resonances. Fluctuations with small initial length scales ($L^i_{100} \lesssim 0.1$ m) converge to a final baryon-to-entropy ratio $(n_b/s)_f \approx 1.1 \times 10^{-5}$. This corresponds to a baryon-to-photon ratio inside the fluctuation of $\eta \approx 8 \times 10^{-5}$ during primordial nucleosynthesis. Fluctuations with initial length scales larger than ($L^i_{100} \gtrsim 1$ m) have less damping, since neutrinos become optically thin on the scale of the fluctuation at low temperatures. The dotted line divides fluctuations containing

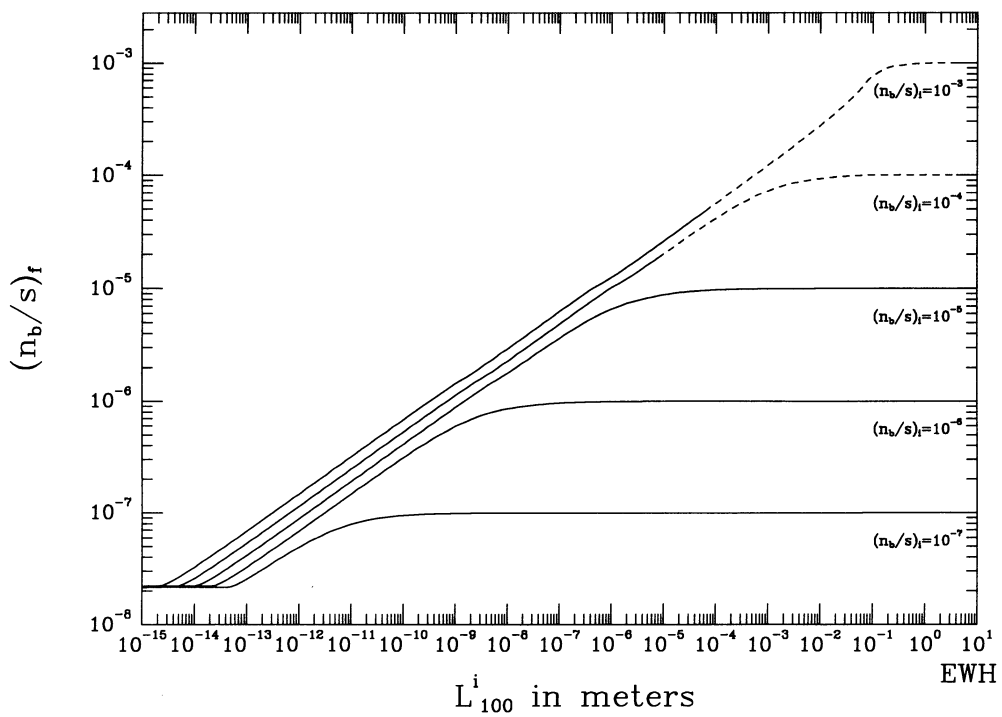

FIG. 7.—Effects of neutrino inflation between the epochs of $T = 100$ GeV and $T = 100$ MeV on entropy fluctuations. We give the final baryon-to-entropy ratio $(n_b/s)_f$ of neutrino-inflated two-zone fluctuations as a function of the initial fluctuation radius L^i_{100} in meters. We use five different initial ($T = 100$ GeV) values, $(n_b/s)_i$. Dashed lines indicate that $(n_b/s)_f$ depends on uncertainties in the QCD equation of state in the strong coupling limit. The approximate horizon scale at $T = 100$ GeV (denoted electroweak horizon [EWH]) is on the far right-hand side of the horizontal scale.

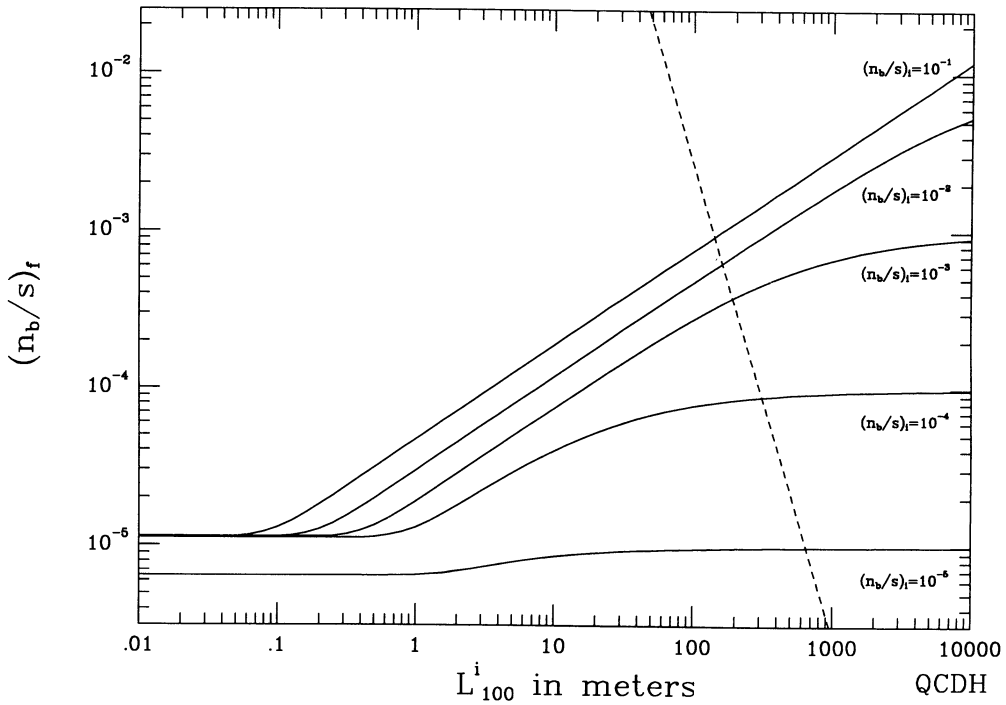

FIG. 8.—Effects of neutrino inflation between the epochs $T = 100$ MeV and $T = 1$ MeV. Notation is as in Fig. 7. We give $(n_b/s)_f$ for fluctuations with initial length scale L^i_{100} in meters and initial ($T = 100$ MeV) amplitude $(n_b/s)_i$ as labeled. The approximate horizon scale at $T = 100$ MeV (QCD horizon [QCDH]) is shown. The dashed line divides fluctuations containing more (*right*) and less (*left*) baryonic mass than the baryon mass in the QCD horizon.

less (*left*) and more (*right*) baryonic mass than to total baryon mass in the horizon at the QCD transition epoch ($T = 100$ MeV).

The effects of neutrino damping on fluctuations between temperatures of $T = 100$ GeV and $T = 1$ MeV are shown in Figure 9. This figure combines results from Figures 7 and 8. Our calculation assumes no fluctuation modification from phase transition effects during the QCD transition epoch. The dashed lines indicate uncertainties in the damping due to equation-of-state uncertainties associated with the strong QCD coupling regime. Even if we were to assume no damping of entropy fluctuations in the strong QCD coupling regime, Figure 9 would be essentially unchanged. Significant damping of entropy fluctuations in the strong QCD coupling limit is unlikely because of the small neutrino mean free path during this epoch. It is evident that neutrino inflation results in a high degree of convergence in the final baryon-to-entropy ratio for a broad range of initial fluctuation amplitudes and length scales. If neutrino inflation operated only in the homogeneous limit, we would expect fluctuations of any initial length scale to converge to the same $(n_b/s)_f$. Most of the neutrino inflation for fluctuations with length scales in the range 10^{-1} m $\gtrsim L^i_{100} \gtrsim 10^{-5}$ m takes place in the homogeneous regime, so that we see a fair degree of convergence in $(n_b/s)_f$ for these fluctuations in Figures 8 and 9.

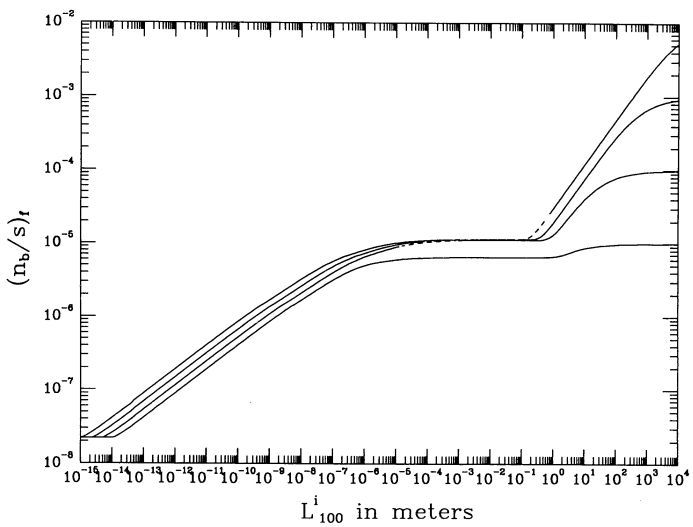

FIG. 9.—Effects of neutrino inflation on entropy fluctuations over the history of the universe between epochs of $T = 100$ GeV and $T = 1$ MeV. Notation is as in Figs. 7 and 8.

How sensitive are these results to our assumptions about the microphysical quantities β and F^*, the expansion rate of the universe, and our simplified treatment of annihilation epochs and phase transitions? When there is sufficient inflation [$\Delta_f \lesssim (1/10)\Delta_i$ with Δ_f, Δ_i the final and initial baryon number overdensities] from high initial temperatures ($T \gtrsim 1$ GeV), we can obtain an approximate analytic result for the final baryon-to-entropy ratio:

$$\left(\frac{n_b}{s}\right)_f \approx 4.5 \times 10^{-7} A \left(\frac{g}{100}\right)^{1/9} \left(\frac{g_\nu}{5.25}\right)^{-4/9} \left(\frac{N_q^4}{N_l + 3N_q}\right)^{1/9} \times \left(\frac{\beta}{2.762}\right)^{1/9} \left(\frac{F^*}{0.747}\right)^{-4/9}, \quad (28a)$$

where

$$A = \left(\frac{\Delta_i}{10^6}\right)^{1/9} \left(\frac{L^i_{100}}{10^{-10}\ \mathrm{m}}\right)^{1/3} \left(\frac{\Omega_b h^2}{0.01}\right)^{1/9}. \quad (28b)$$

Quantities in equations (28a) and (28b) which are temperature-dependent (e.g., g, N_q, and N_l) should be taken to be their values at the epoch where the neutrino mean free path is of the order of the fluctuation length scale. The value of $(n_b/s)_f$ in equation (28) is only very weakly dependent on the mean free path ($\sim\beta$), the total statistical weight (g), and the number of relativistic quarks N_q and leptons N_l at temperature T. Furthermore, the effects of neutrino inflation are clearly insensitive to the average baryon-to-photon ratio ($\sim\Omega_b h^2$) and the initial overdensity Δ_i. There is more significant dependence of the final ratio $(n_b/s)_f$ on the number of heat transporters (g_ν) and the efficiency of the heat transport ($\sim F^*$). Uncertainties in the precise QCD transition temperature will not affect the outcome of neutrino inflation significantly unless the QCD transition temperature is very low ($T < 100$ MeV). Neutrino inflation is not very efficient after the QCD transition if there are large numbers of thermally produced baryon-antibaryon pairs (Fig. 5), as would be the case for a QCD transition temperature $T > 100$ MeV. We do not expect the annihilation of pions and muons to modify our results substantially.

2.2. *Photon Inflation and Hydrodynamic Expansion*

At temperatures lower than $T \approx 30$ keV baryon-to-entropy fluctuations are efficiently damped by photon diffusion and hydrodynamic expansion against photon Thomson drag (Alcock et al. 1990). The number density of $e^\pm$ pairs in the universe remains large compared with the number density of ionization electrons until the temperature drops below about $T \approx 30$ keV. The photon mean free path or, equivalently, the total photon transport cross section is determined by photon-electron and photon-positron scattering. When the pairs finally annihilate, we expect a substantial increase in the photon mean free path. If the photon mean free path becomes of the order of or larger than the fluctuation size L, then the photons go from optically thick to optically thin on this scale. In the optically thin limit all temperature differences between the inside and outside of the fluctuation are erased. In this case we can no longer use radiation pressure to balance the difference in baryon pressure between the inside and the outside of the fluctuation. The unbalanced baryon pressure leads to hydrodynamic expansion of the fluctuation.

In the limit where Klein-Nishina corrections are small ($T \lesssim m_e$), the photon mean free path is

$$l_{\gamma e} \approx \frac{1}{\sigma_T n_{e^\pm}}, \tag{29}$$

where $\sigma_T \approx 6.7 \times 10^{-25}$ cm^2 is the Thomson cross section, and $n_{e^\pm} = n_{e^-} + n_{e^+}$ is the number density of electrons plus positrons. At temperatures above the electron rest mass the photon-electron scattering cross section is smaller than the Thomson cross section. However, the photon mean free path is still small in this case, since there are a large number of thermally produced charged particles. Figure 10 shows the photon mean free path $l_\gamma^{100} = l_\gamma/R$ for temperatures below $T = 1$ MeV. Figure 3 for $R(T)$ can be used to convert comoving distances into proper distances.

In Figure 10 we show the photon mean free path for three different proton fluctuation amplitudes Δ_p. The proton density, n_p, which equals the net electron density from charge neutrality, is just

$$n_p = \bar{n}_b \Delta_p . \tag{30}$$

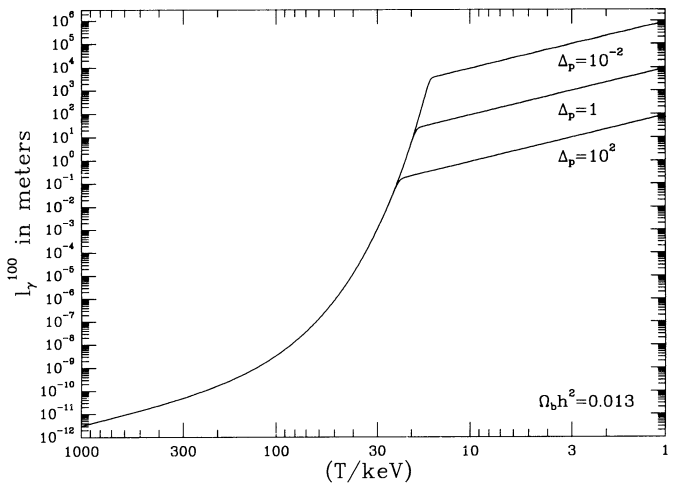

FIG. 10.—Photon mean free path $l_\gamma^{100} = l_\gamma/R$ in meters as a function of temperature. Results are displayed for three different proton fluctuation amplitudes Δ_p. A fraction of the closure density in baryons, $\Omega_b = 0.013\ h^{-2}$, has been assumed.

In Figure 10 we neglect alpha particles. The photon mean free path rises sharply during the epoch of e^+e^- annihilation until the number density of thermal e^+e^- pairs drops below the net electron density at temperatures around $T \approx 30$ keV. After e^+e^- annihilation the photon mean free path depends only on the net electron density and so tracks the proton density across a fluctuation. Thus the photon mean free path can vary by several orders of magnitude across a fluctuation. A large photon mean free path contributes to efficient damping of small-scale nonlinear entropy fluctuations. We consider two limits for damping of fluctuations by this process which are the analogs of the two limits considered for neutrino inflation.

Fluctuations expand as a result of diffusive photon heat transport when the photon mean free path is smaller than the fluctuation length scale $l_\gamma < L$. In this limit the heat diffusion equation (14) applies, with the photon heat diffusion constant D_γ approximately given by

$$D_\gamma \approx \frac{g_t}{g_{\rm eff}} l_{\gamma e}, \tag{31}$$

where g_t is the statistical weight of heat-transporting particles (photons, $g_t = 2$), and $g_{\rm eff}$ is the statistical weight of relativistic particles still "coupled" to the material in the fluctuation (γ, $e^\pm$). Using equations (14) and (16), we can obtain an approximate damping timescale. We take this to be τ_γ, the time to double the size of a square wave entropy fluctuation by photon heat advection,

$$\tau_\gamma^{-1} \approx \frac{1}{5 \times 10^3\ {\rm s}} \left(\frac{L_{100}}{\rm m}\right)^{-2} \left(\frac{T}{10\ {\rm keV}}\right)^{-1} \left(\frac{2\Delta_p + 3\Delta_{^4{\rm He}}}{\Delta_p + 2\Delta_{^4{\rm He}}}\right), \tag{32}$$

where L_{100} is the comoving fluctuation length as before, and $\Delta_{^4{\rm He}}$ is the ^{4}He density defined in a manner analogous to Δ_p in equation (30). Since we here deal with temperatures well within the nucleosynthesis epoch, we must allow for a significant ^{4}He mass fraction. Equation (32) assumes complete annihilation of e^+e^- pairs and thus applies only at low temperatures $T \lesssim 20$ keV. The denominator in the last factor in equation (32) arises

from the net electron density within the fluctuation, whereas the numerator is related to the temperature deviation δ in the fluctuation.

When the photons become optically thin on the scale of the fluctuation ($l_\gamma > L$), the temperature across the fluctuation becomes uniform and the fluctuation disintegrates by hydrodynamic expansion. The overpressure due to extra baryons and electrons within the fluctuation will drive collective fluid expansion out of the fluctuation. However, protons moving through an isotropic photon gas will experience a drag force proportional to the fluid velocity. As seen from the proton rest frame, the photon flux against the direction of motion is slightly higher than the photon flux from the opposite direction. Electrons are dragged along by the protons through electric forces. These electrons Compton-scatter more often in head-on collisions transferring some net momentum to the photon gas. This leads to the Thomson drag force on the moving fluid, $F = (4/3)\sigma_T \varepsilon_\gamma (v/c)$ (Peebles 1971). Because of this drag force the expanding fluid will reach a terminal peculiar velocity $v = dr_{100}/dt$,

$$v \approx \frac{3}{4\sigma_T \varepsilon_\gamma n_e} \frac{1}{R^2} \frac{dP}{dr_{100}}, \tag{33}$$

where dP/dr_{100} is the radial pressure gradient, r_{100} is the radial coordinate as measured on our comoving scale, ε_γ is the energy density in photons, and $n_e = n_{e^-} - n_{e^+}$ is the net electron density. We find for the pressure exerted by baryons and electrons below $T \approx 30$ keV

$$P \approx \bar{T}\bar{n}_b \left\{ \sum_i \Delta_i + \left[n_{\rm pair}^{*2} + \left(\sum_i Z_i \Delta_i \right)^2 \right]^{1/2} - n_{\rm pair}^* \right\}, \tag{34}$$

with the sum running over all nuclei i with nuclear charge Z_i. In this expression the e^+e^- pair density divided by $\bar{n}_b$ is

$$n_{\rm pair}^* \approx \frac{1}{\bar{n}_b} \frac{1}{2} \left(\frac{2}{\pi} \right)^{3/2} (m_e T)^{3/2} \exp\left(-\frac{m_e}{T} \right) \left(1 + \frac{15}{8} \frac{T}{m_e} \right), \tag{35}$$

which is similar to equation (21) for baryons. The timescale to double the size of a square wave fluctuation by hydrodynamic expansion can be obtained from a characteristic fluid velocity and a characteristic fluctuation length L_{100}. This time scale is roughly $\tau_h \approx L_{100}/v$. After complete e^+e^- annihilation, we find

$$\tau_h^{-1} \approx \frac{1}{2.4 \times 10^3 \text{ s}} \left(\frac{L_{100}}{\text{m}} \right)^{-2} \left(\frac{T}{10 \text{ keV}} \right)^{-1} \left(\frac{2\Delta_p + 3\Delta_{^4\text{He}}}{\Delta_p + 2\Delta_{^4\text{He}}} \right), \tag{36}$$

with the notation as before. This hydrodynamic expansion time-scale is similar to the inflation timescale from diffusive photon heat transport in equation (32). It is important to note that the damping timescales for diffusive photon heat flow and hydrodynamic expansion are independent of fluctuation amplitude. In Figure 11 we show damping rates for diffusive photon inflation, τ_γ^{-1} (*dashed line*), and hydrodynamic expansion, τ_h^{-1} (*dash-dot line*), for a fluctuation with $L_{100} = 1$ m. In this figure we also show the reciprocal of the Hubble time, $\tau_H^{-1} \approx (8\pi G\varepsilon/3)^{1/2}$ (*solid line*) between temperatures of $T = 100$ keV and $T = 1$ keV. Damping timescales are shorter than the Hubble time at this epoch for fluctuations smaller than $L_{100} \lesssim 1$ m and for temperatures below $T \approx 30$ keV. We conclude that small inhomogeneities will disintegrate rapidly below $T \approx 30$ keV. Larger fluctuations, $L_{100} > 1$ m, will disintegrate at somewhat lower temperatures.

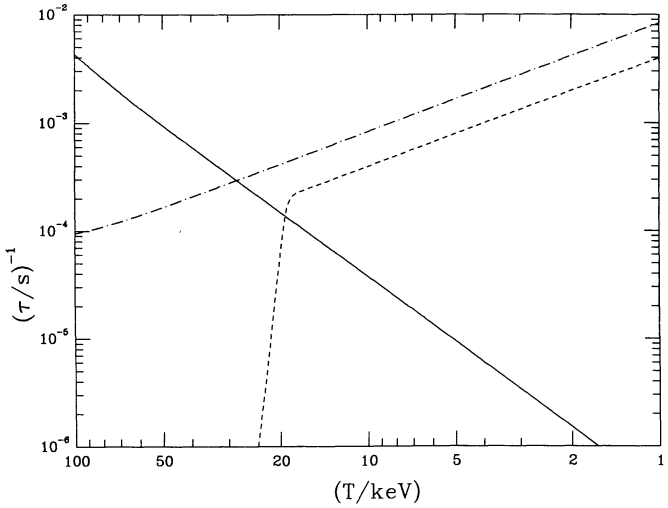

FIG. 11.—Fluctuation damping rates due to diffusive photon inflation (*dashed line*) and hydrodynamic expansion against Thomson drag (*dash-dot line*), and the Hubble expansion rate (*solid line*), are given as functions of temperature. The fluctuation length is taken as $L_{100} = 1$ m.

In this work we ignore all nonspherical dissipative modes (e.g., convection, dendritic instabilities, and Rayleigh-Taylor instabilities). This approximation is valid over all the range of conditions we consider except possibly at very late times when rapid hydrodynamic expansion against Thomson drag occurs. Simple estimates show that the acceleration at these times is so small that the surface of an expanding fluctuation is Rayleigh-Taylor–stable.

2.3. *Baryon Diffusion*

High-amplitude subhorizon-scale baryon-to-entropy fluctuations in the early universe are modified considerably by baryons diffusing through the primordial plasma (Applegate et al. 1987). The baryon diffusion equation in spherical comoving coordinates, $r_{100} = r/R$, is

$$\frac{\partial \Delta_i}{\partial t} = \frac{1}{r_{100}^2} \frac{\partial}{\partial r_{100}} \left(\frac{D_i}{R^2} r_{100}^2 \frac{\partial}{\partial r_{100}} \Delta_i \right) - \sum_i f_{ij}(T) \Delta_j, \tag{37}$$

where Δ_i is the ratio of the number density of nucleus i to the total baryon number density, and D_i is the diffusion constant for the ion corresponding to nucleus i. We include in equation (37) a source term representing changes in the nuclear abundances due to nuclear reactions, so that the coefficients f_{ij} represent nuclear reaction rates. Up to a numerical factor of order unity, the baryon diffusion constant D_i for nucleus i is

$$D_i \approx \frac{1}{3} v_i l_i = \frac{1}{3} v_i \frac{1}{\sigma_{ik} n_k}, \tag{38}$$

with v_i the thermal baryon velocity, l_i the baryon mean free path, σ_{ij} the cross section for the scattering of nucleus i on particle k, and n_k the number density of particle k.

In Table 1 we list the baryon diffusion constants of neutrons and protons, as well as the heat diffusion constant for photons in the early universe (Applegate et al. 1987; Banerjee & Chitre 1991; Gould 1993). We show baryon diffusion constants for the scattering of baryons on individual particle species k. The effective baryon diffusion constant of nucleus i in the primor-

TABLE 1

DIFFUSION CONSTANTS, CROSS SECTIONS, AND COSMOLOGICAL IMPORTANCE OF SCATTERING PROCESSES

Scattering Process	Diffusion Constant[a]	Cross Section	Cosmological Importance	In Code	Reference
$n + e \rightarrow n + e$	$D^* \approx (9.1 \times 10^2\ \mathrm{m^2\ s^{-1}})(T/\mathrm{MeV})^{1/2}(n_e/\mathrm{MeV}^3)^{-1}$, $n_e = n_{e^-} + n_{e^+}$	$\sigma_{ne} \approx 8.0 \times 10^{-35}\ \mathrm{m^2}$	$T > 100$ keV and $\eta < 3 \times 10^{-8}$	Yes	Applegate et al. 1987
$n + p \rightarrow n + p$	$D \approx (3\pi^{1/2}/4)(c/n_p)(1/\sigma_{np})(T/m_p)^{1/2}$ $\approx (2.65 \times 10^{-3}\ \mathrm{m^2\ s^{-1}})R^3(T/\mathrm{MeV})^{1/2}(\Delta_p \Omega_b h^2)^{-1}$	$\sigma_{np} \approx 2.0 \times 10^{-27}\ \mathrm{m^2}$	$T < 100$ keV or $\eta > 3 \times 10^{-8}$, all T	Yes	Banerjee & Chitre 1991
$n + \gamma \rightarrow n + \gamma$		$\sigma_{n\gamma} \approx 3.4 \times 10^{-40}\ \mathrm{m^2} \times (T/\mathrm{MeV})^2$	None	No	Gould 1993
$p + e \rightarrow p + e$	$D \approx (\frac{3}{8})(\pi/2)^{1/2}(c/n_e)(1/\sigma_{pe})(T/m_e)^{1/2}$	$\sigma_{pe} \approx 2.6 \times 10^{-29}\ \mathrm{m^2} \times (T/\mathrm{MeV})^{-2} \log \delta$, $\delta = \lambda_D/\lambda_{th}$	1 MeV $> T >$ 40 keV and $T < 0.1$ keV	No	Banerjee & Chitre 1991
$p + \gamma \rightarrow p + \gamma$	$D \approx (\frac{3}{8})(\pi/2)^{1/2}(c/n_\gamma)(1/\sigma_{p\gamma})(T/m_p)^{1/2}$	$\sigma_{p\gamma} \approx 2 \times 10^{-35}\ \mathrm{m^2}$	None	No	Banerjee & Chitre 1991
$e + \gamma \rightarrow e + \gamma$	$D^* \approx (0.2\ \mathrm{m^2\ s^{-1}})(T/\mathrm{MeV})^{-5/2}$	$\sigma_{e\gamma} = \sigma_T \approx 6.7 \times 10^{-29}\ \mathrm{m^2}$	40 keV $> T > 0.1$ keV (proton diffusion)	Yes	
$\gamma + e \rightarrow \gamma + e$	$D^* \approx (3.4 \times 10^{-2}\ \mathrm{m^2\ s^{-1}})(n_e/\mathrm{MeV}^3)^{-1}$	σ_T	$T < 30$ keV (heat diffusion)	Yes	

[a] An asterisk following D means that D was estimated assuming $D \approx vl \approx v/(\sigma n_{sc})$.

dial plamsa due to all scattering is

$$\frac{1}{D_i} = \sum_j \frac{1}{D_{ij}} . \tag{39}$$

Table 1 also displays the relevant cross sections and the relative cosmological importance of individual scattering processes.

Neutrons diffuse relatively easily through the primordial plasma. At temperatures above $T \approx 100$ keV, neutron diffusion is limited by magnetic moment scattering on electrons and positrons. However, at lower temperatures ($T \lesssim 100$ keV), or in high-density fluctuations with a local baryon-to-photon ratio $\eta \gtrsim 3 \times 10^{-8}$, neutron diffusion is limited by nuclear scattering on protons. Thus, the effective damping of high-amplitude fluctuations ($\Delta \gg 1$) by baryon diffusion is a nonlinear process, since neutron diffusion is less efficient for a higher proton density.

Before the freeze-out from weak equilibrium ($T \approx 1$ MeV) there is no segregation between neutrons and protons, and baryons only diffuse efficiently during the fraction of time they spend as neutrons. After weak equilibrium freeze-out, protons and neutrons diffuse independently, and, since protons and neutrons have different diffusion constants, the result will be spatial segregation of these species. Proton diffusion has negligible effects above $T \approx 30$ keV, except for the very smallest fluctuations $L_{100} \ll 1$ m. However, such small fluctuations are damped efficiently by baryon diffusion before weak freeze-out.

For temperatures above $T \approx 40$ keV Coulomb scattering of protons off electrons and positrons dominates the proton diffusion constant. This is because protons move through the plasma as independent particles; in particular, protons do not drag along electrons. The proton electric charge is shielded by plasma electrons, since the Debye screening length is much smaller than a typical interparticle spacing (Applegate et al. 1987). The diffusivity of heavy nuclei for temperatures above $T \approx 40$ keV should also be limited by Coulomb scattering of the nuclei off electrons and positrons. A simple estimate for the diffusion constant of nuclei relative to that of protons can be easily obtained from equation (38). The diffusivity of nuclei should be suppressed relative to the diffusivity of protons because of a larger Coulomb cross section for the scattering of e^+e^- off nuclei and a smaller thermal velocity of the nuclei. For a nucleus with nuclear charge Z_i and nucleon number A_i, the Coulomb cross section is Z_i^2 times larger than that for protons and the thermal velocity is $1/A_i$ times smaller than the proton thermal velocity. This leads to a suppression factor of the diffusivity of nuclei relative to that for protons of $(1/Z_i^2 A_i)$.

In the temperature range 40 keV $\gtrsim T \gtrsim 0.1$ keV, Compton scattering of electrons off photons limits proton diffusion. In contrast to the situation at higher temperatures, the dilute e^+e^- plasma at lower temperatures is inefficient in shielding isolated charges. Charge neutrality then requires a proton and an electron to move together, and the effective proton diffusion constant is the smaller of the electron diffusion constant and the proton diffusion constant. Nuclei have to drag along a cloud of Z_i electrons. Naively, we may expect the diffusion constant for nuclei to be suppressed by a factor of $1/Z_i$ relative to that of the proton-electron system. This is because there are Z_i as many electrons scattering off photons, and the probability of a change in momentum of the nucleus-electron cloud system is Z_i times as large as that for the proton-electron system. Below $T \approx 0.1$ keV proton and nucleus diffusion is again limited by Coulomb scattering as a result of the temperature-dependent increase of the Coulomb cross section.

It is instructive to compute the diffusion length of baryons, $d(t)$. This is the rms distance a baryon diffuses in time t. The diffusion length $d_{100} = d/R$ in the early universe becomes (Applegate et al. 1987)

$$d_{100}(t) = \left[\frac{6}{R^2}\int_0^t D(t')dt'\right]^{1/2} , \tag{40}$$

and a simple integration through the e^+e^- annihilation epoch yields the results displayed in Figure 12. In this figure we show d_{100}^n for neutrons as a function of the temperature of the universe for three different local baryon-to-photon ratios ($\eta = 1 \times 10^{-4}$, $\eta = 3.5 \times 10^{-10}$, and $\eta = 3.5 \times 10^{-12}$). This figure also shows d_{100}^p for protons. It is evident that baryon diffusion is inhibited in large-amplitude fluctuations.

An approximate timescale to double the size of a square wave fluctuation by baryon diffusion is

$$\tau_b \approx \frac{L^2}{D_b} , \tag{41}$$

where D_b is the relevant baryon diffusion constant and L is the fluctuation length scale. Note that the damping timescale is

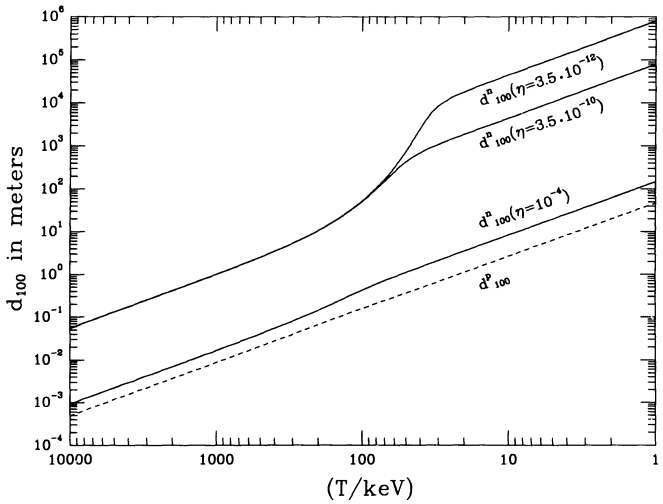

FIG. 12.—Proton (*dashed line*) and neutron (*solid line*) diffusion lengths $d_{100} = d/R$ in meters given as functions of temperature. We assume that the diffusive random walk starts at $T = 100$ MeV. The neutron diffusion length is shown for three different baryon-to-photon ratios η.

independent of the fluctuation amplitude Δ provided that D_b is independent of Δ. In Figure 13 we compare the timescales for neutron diffusion limited by magnetic moment scattering (*short-dashed line*), neutron diffusion limited by nuclear scattering in a fluctuation with $\eta = 6 \times 10^{-9}$ (*dash-dot line*), and proton diffusion (*long-dashed line*) to the Hubble time (*solid line*) between temperatures of $T = 10$ MeV and $T = 10$ keV. For a fluctuation length $L_{100} \gtrsim 1$ m we find proton diffusion to have negligible effects above $T \approx 20$ keV. Neutron diffusion is seen to be dependent on the local proton density. A high density fluctuation with characteristic interior baryon-to-photon ratio $\eta \approx 10^{-4}$ and fluctuation length $L_{100} \approx 1$ m will not be much affected by neutron diffusion whenever the temperature is above $T \approx 50$ keV.

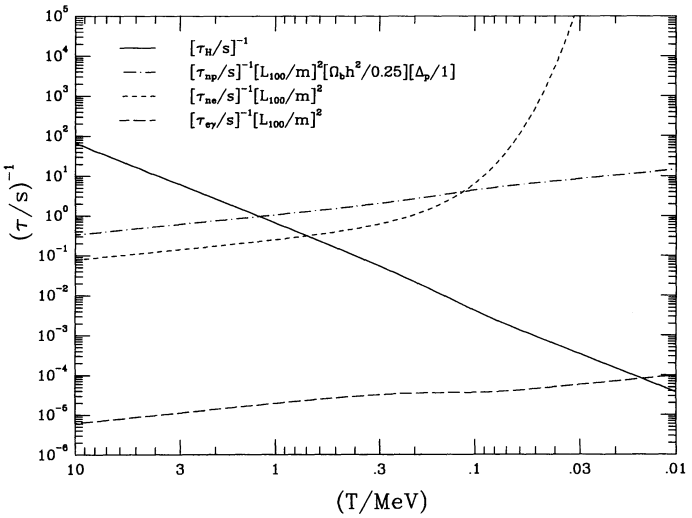

FIG. 13.—Inverse of fluctuation damping timescales from baryon diffusion, displayed as functions of temperature. Shown are the neutron diffusion damping rate limited by *ne* scattering (*short-dashed line*), neutron diffusion damping rate limited by *np* scattering (*dash-dot line*), and proton diffusion damping rate limited by *eγ* scattering (*long-dashed line*). For comparison the Hubble expansion rate (*solid line*) is given. The key in the upper left-hand corner of the figure displays the dependence of the different timescales on assumed fluctuation radius $L_{100} = 1$ m, average fraction of closure density in baryons $\Omega_b = 0.25\,h^{-2}$, and proton fluctuation amplitude $\Delta_p = 1$.

3. EVOLUTION OF ENTROPY FLUCTUATIONS IN THE EARLY UNIVERSE

3.1. *Numerical Simulation*

We have simulated the evolution of high-amplitude baryon-to-entropy fluctuations between temperatures of $T = 100$ MeV and $T = 10$ keV. The numerical simulation presented here does not include the synthesis of elements below temperatures of $T \approx 100$ keV. We evolve a spherical region of the universe, which contains an initially Gaussian-shape fluctuation at its center. We assume that the horizon volume is filled with such spherical regions, so that the mean separation of fluctuation centers is approximately twice the cell radius. These assumptions lead to reflective boundary conditions for baryon number flux and heat flux at the spherical cell's edge. We represent a fluctuation by a Lagrangian grid with 60 zones in the spherical cell.

Baryon diffusion, neutrino inflation, and photon inflation are treated in a simple intuitive manner. Initially, we take each zone to be in pressure equilibrium. This pressure equilibrium configuration is characterized by a temperature deviation δ^0 and proton (neutron) fluctuation amplitudes Δ^0_p (Δ^0_n) in each zone. Diffusive processes during a time interval dt will change the temperature differences in each zone by $\delta^0 \rightarrow \delta^1$, and the baryon densities by $\Delta^0_{p,n} \rightarrow \Delta^1_{p,n}$. This will perturb the existing pressure equality, and will result in an adiabatic expansion (contraction) of zones, until pressure equilibrium is reestablished for new zone values of δ, Δ_p, and Δ_n. The simple algorithm used here has the advantage of being easily tested against our analytic calculations for a two-zone square wave fluctuation.

To obtain the changes in energy density from diffusive processes in zone i during a time interval dt, we rewrite the heat diffusion equation (14) in integral form, which yields

$$\delta^1_i = \delta^0_i + \frac{dt}{x_i^3 - x_{i-1}^3} \times \left(6 \frac{D}{R^2} x_i^2 \frac{\delta^0_{i+1} - \delta^0_i}{x_{i+1} - x_{i-1}} - 3 \int_0^{x_{i-1}} x^2 \frac{d\delta}{dt}\, dx \right), \quad (42)$$

where x_i is the outer boundary of the ith zone. In this expression x_i is measured on our comoving $T = 100$ MeV scale, so that x_i is shorthand notation for x^i_{100}. For homogeneous neutrino heat transport we find a change in the energy density in time interval dt given by

$$\delta^1_i = \delta^0_i \left(1 - dtF^* \frac{g_\nu}{g_{\rm eff}} \frac{1}{l_\nu} \right). \quad (43)$$

For this special case the heating is uniform across all zones i in the fluctuation.

Changes in baryon density due to baryon diffusion are obtained from an integral diffusion equation similar to equation (42). However, efficient neutron diffusion at low temperatures necessitates the use of an implicit algorithm. We replaced neutron densities at time t_0 on the right-hand side of equation (42) by neutron densities at time t_1. The resulting matrix equation can be solved by the standard methods of Gaussian elimination and back-substitution. In addition, we added weak interaction conversion between neutrons and protons. Weak reaction rates, as well as the evolution of the scale factor R, temperature T, and statistical weight g are

treated as in the primordial nucleosynthesis code of Wagoner, Fowler, & Hoyle (1967) as updated by Kawano (1992).

Having computed the changes in energy and baryon content of the fluctuation in the time interval dt, from heat transport, baryon diffusion, and weak interactions, we then allow each zone to expand adiabatically to a new pressure equilibrium. For this purpose we fix the common pressure in all zones after adiabatic expansion to equal the average pressure in the whole spherical cell in which the simulation is performed. Thus, it is easy to compute the fractional volume change of zone i, $(dV/V)_i$, needed to attain pressure equilibrium

$$\left(\frac{dV}{V}\right)_i \approx 3(\delta_i^1 - \delta_i^0) . \tag{44}$$

We can leave out changes in the baryon density in equation (44), since the associated changes in baryon pressure in different zones are negligible compared with the pressure changes from heat transport. This approximation is good, since the baryon-to-photon ratio is everywhere small in our calculation.

Both photons and neutrinos eventually will decouple on the scale of the fluctuation. The assumption of pressure equilibrium breaks down when the photons decouple from the fluctuation ($l_\gamma > L$). The simulation of the hydrodynamic expansion of a fluctuation is nontrivial, since the photon mean free path l_γ varies strongly over the spherical cell radius. We encounter situations where photons are still in the optically thick regime in high-density regions of the fluctuation but are in the optically thin regime in lower density regions. In this case the damping of the fluctuation proceeds by diffusive heat transport in the core region of a fluctuation where the baryon density is high, and by hydrodynamic expansion near the boundary of the fluctuation. Numerical simulation of this process requires the introduction of independent sets of photon zones and baryon zones.

Neutrinos are easier to treat. The neutrino mean free path l_ν is independent of the baryon overdensity Δ, and neutrinos go quickly from the optically thick limit to the optically thin limit. Therefore, it is a fairly accurate approximation to switch from diffusive neutrino heat transport to homogeneous neutrino heat transport when the neutrino mean free path becomes larger than the width a of the Gaussian fluctuation.

In the following we will summarize the results of our numerical simulation. Figures 14–16 show the evolution of three sample high-density spherically condensed Gaussian entropy fluctuations for temperatures between $T = 100$ MeV and $T = 10$ keV. The initially Gaussian fluctuations are characterized by four quantities: the average baryon-to-photon ratio η (equivalently $\Omega_b h^2$) within the spherical simulation volume, the radius of the spherical simulation volume L_{100}^s, the ratio of the radius L_{100}^s to the Gaussian width of the baryon density distribution a, and the ratio of the baryon density at the core of the fluctuation, n_b^H, to the baryon density at the edge of the simulation volume, n_b^L, $\Lambda = (n_b^H/n_b^L)$. For each sample we show nine evolution snapshots of the fluctuation at different temperatures. We plot the logarithm of the neutron and proton fluctuation amplitudes ($\log_{10} \Delta_n$ and $\log_{10} \Delta_p$) as functions of the radius $r_{100} = r/R$. We reference all proper lengths to the values they would have at $T = 100$ MeV to remove the effects of the overall Hubble expansion. Solid lines indicate the local proton fluctuation amplitude, Δ_p, whereas dotted lines indicate the local neutron fluctuation amplitude, Δ_n.

In Figure 14 the effects of neutrino inflation are evident. Very high amplitude fluctuations with an initial central baryon-to-entropy ratio $(n_b/s)_i \gtrsim 1.5 \times 10^{-5}$ are damped to a characteristic flat-top fluctuation with final baryon-to-entropy ratio $(n_b/s)_f \approx 1.5 \times 10^{-5}$ (corresponding to an ultimate baryon-to-photon ratio of $\eta_f \approx 8 \times 10^{-5}$). The limiting amplitude is attained between temperatures of $T \approx 100$ MeV and $T \approx 20$ MeV, depending on initial fluctuation parameters.

The modifications of fluctuations due to neutron diffusion are evident in all three sample evolution plots. Figure 16 illustrates that small-scale fluctuations, $L \lesssim 0.5$ m, are almost completely homogenized and damped out before the onset of primordial nucleosynthesis at $T \approx 100$ keV.

Photon inflation and the hydrodynamic expansion of fluctuations at low temperatures are seen to be rapid and rather violent events. This is evident in Figure 15. Between temperatures of $T \approx 35$ keV and $T \approx 10$ keV these processes lower the core proton density of fluctuations by several orders of magnitude. The effects of proton diffusion at low temperatures ($T \approx 20$ keV) add to the violent decay of such small-scale fluctuations.

4. CONCLUSIONS

In the present study we have investigated the evolution of fluctuations in the baryon-to-photon ratio (entropy fluctuations) between the end of a cosmic electroweak phase transition at $T \approx 100$ GeV and the end of primordial nucleosynthesis at $T \approx 5$ keV. Our study focused on nonlinear subhorizon-scale fluctuations. Entropy fluctuations may result from an epoch of the early universe where there is a departure from local thermodynamic equilibrium such as a first-order electroweak phase transition or an inflationary period. We have shown that entropy fluctuations evolve rapidly to an isobaric character.

Fluctuations are found to damp by five different physical processes: neutrino inflation in the diffusive and homogeneous limits, photon inflation and hydrodynamic expansion, and baryon diffusion.

Neutrino inflation provides the dominant damping of entropy fluctuations between temperatures of $T \approx 100$ GeV and $T \approx 1$ MeV. Fluctuations are damped by neutrino heat transport in such a way that almost any initial fluctuation amplitude converges to a generic final fluctuation amplitude. Fluctuations of high initial amplitude and with an initial fluctuation length $L_{100} \lesssim 10^{-14}$ m become damped to a characteristic baryon-to-entropy ratio $(n_b/s) \approx 2 \times 10^{-8}$. These fluctuations evolve to this amplitude between $T \approx 100$ GeV and $T \approx 1$ GeV, depending on their initial characteristics. Fluctuations in the length scale regime 10^{-5} m $\lesssim L_{100} \lesssim 10^{-1}$ m are damped to a characteristic baryon-to-entropy ratio $(n_b/s) \approx 1.1 \times 10^{-5}$ (corresponding to an ultimate baryon-to-photon ratio $\eta \approx 8 \times 10^{-5}$) at an epoch between $T \approx 100$ MeV and $T \approx 1$ MeV.

The effects of photon inflation and hydrodynamic expansion on entropy fluctuations are shown to be significant at temperatures below $T \approx 30$ keV, corresponding to the approximate completion of e^+e^- annihilation. Fluctuations with an initial fluctuation length $L_{100} \lesssim 1$ m are almost completely erased by these processes by the time the temperature has reached $T \approx 20$ keV.

Our numerical calculations of fluctuation evolution include all relevant diffusive and hydrodynamic damping processes. We do not include any modifications due to nuclear reactions here. Clearly our results have important implications for pri-

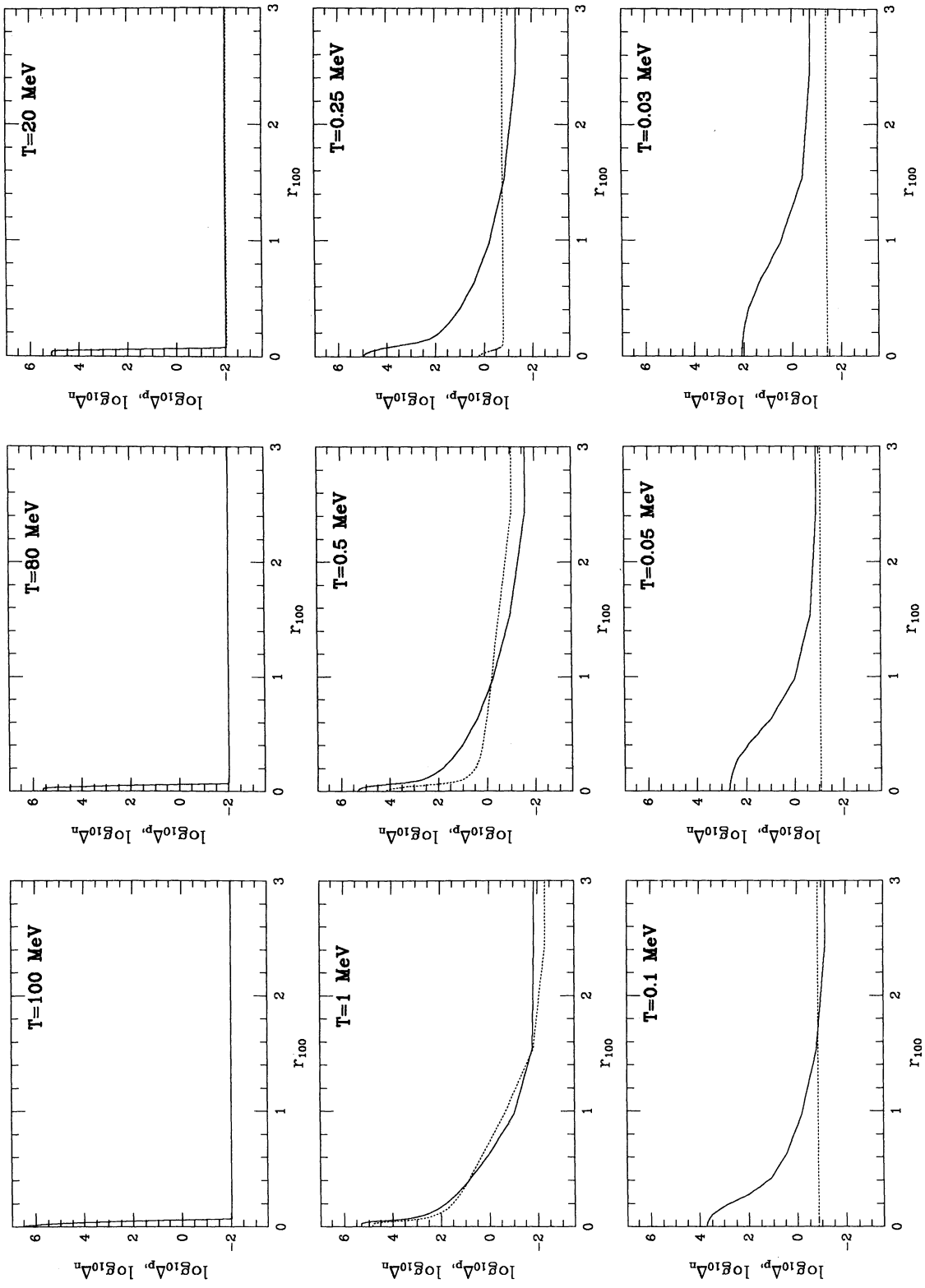

$$\Omega_b=0.013*h^{-2},\ l^s_{100}=3m,\ l^s_{100}/a=200,\ \Lambda=(n_b^H/n_b^L)=3\times10^8$$

FIG. 14.—Evolution of a sample entropy fluctuation over the history of the universe between epochs $T = 100$ MeV and $T = 30$ keV. We show nine evolution snapshots at different temperatures T. Each evolution snapshot displays the logarithm of the proton fluctuation amplitude $\log_{10}\Delta_p$ (*solid line*) and the logarithm of the neutron fluctuation amplitude $\log_{10}\Delta_n$ (*dotted line*) as functions of radial coordinate $r_{100} = r/R$ in meters. The assumed initial fluctuation characteristics are displayed at the bottom of the plots.

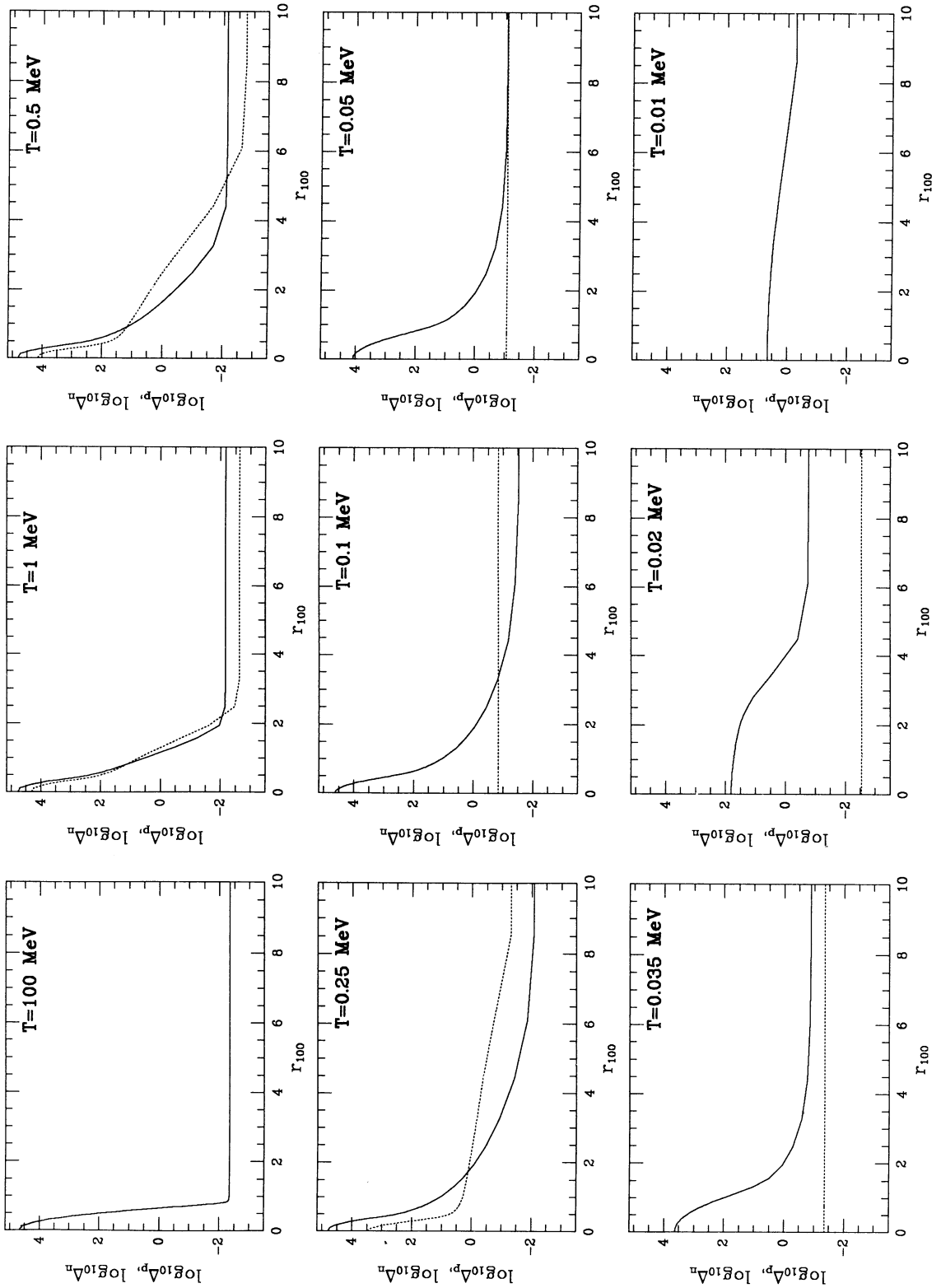

$\Omega_b=0.013*h^{-2}$, $l^s_{100}=10m$, $l^s_{100}/a=50$, $\Lambda=(n_b^H/n_b^L)=10^7$

FIG. 15.—Same as Fig. 14, but with different initial fluctuation characteristics as shown

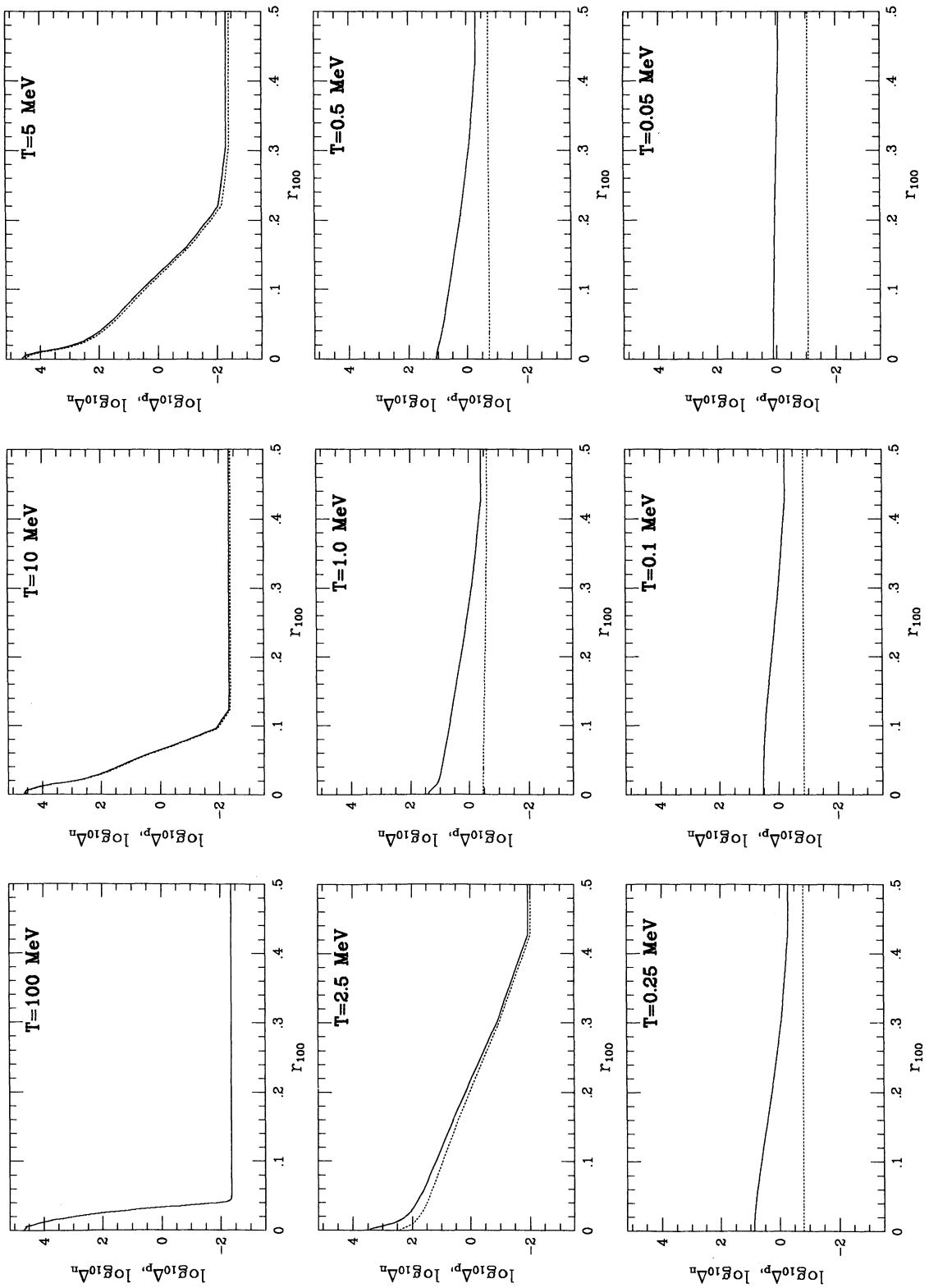

FIG. 16.—Same as Fig. 14, but with different initial fluctuation characteristics as shown

mordial nucleosynthesis yields in inhomogeneous cosmologies. We will address these issues in future work.

The authors wish to thank the Institute of Geophysics and Planetary Physics at Lawrence Livermore National Laboratory, and acknowledge useful discussions with C. R. Alcock, G. J. Mathews, and B. S. Meyer. We also wish to thank L. H. Kawano. This work was supported by NSF grant PHY-9121623 and IGPP grant 93-22.

REFERENCES

Alcock, C. R., Dearborn, D. S., Fuller, G. M., Mathews, G. J., & Meyer, B. S. 1990, Phys. Rev. Lett., 64, 2607
Alcock, C. R., Fuller, G. M., & Mathews, G. J. 1987, ApJ, 320, 439
Applegate, J. H. 1991, Nucl. Phys. A, 527, 195c
Applegate, J. H., & Hogan, C. J. 1985, Phys. Rev. D, 31, 3037
Applegate, J. H., Hogan, C. J., & Scherrer, R. J. 1987, Phys. Rev. D, 35, 1151
Banerjee, B., & Chitre, S. M. 1991, Phys. Lett. B, 258, 247
Brown, F. R., Butler, F. P., Hong Chen, & Christ, N. H. 1990, Phys. Rev. Lett., 65, 2491
Cohen, A., Kaplan, D., & Nelson, A. 1990, Phys. Lett. B, 245, 561
———. 1991a, Nucl. Phys. B, 349, 727
———. 1991b, Phys. Lett. B, 263, 86
Dine, M., Huet, P., Singleton, R., & Susskind, L. 1991, Phys. Lett. B, 257, 351
Dolgov, A., & Silk, J. 1993, Phys. Rev. D, 47, 4244
Fuller, G. M., Jedamzik, K., Mathews, G. J., & Olinto, A. 1993, Phys. Lett. B, submitted
Fuller, G. M., Mathews, G. J., & Alcock, C. R. 1988, Phys. Rev. D, 37, 1380
Gould, R. J. 1993, ApJ, 417, 12
Hagedorn, R. 1971, Thermodynamics of Strong Interactions (CERN Lecture Notes, CERN 71-12)
Heckler, A., & Hogan, C. J. 1993, Phys. Rev. D, 47, 4256
Hogan, C. J. 1978, MNRAS, 185, 889
———. 1993, ApJ, 415, L63
Jedamzik, K., Fuller, G. M., & Mathews, G. J. 1994, ApJ, 423, 50
Kajantie, K., & Kurki-Suonio, H. 1986, Phys. Rev. D, 34, 1719
Kawano, L. H. 1992, Fermilab-Pub-92/04-A, preprint
Kirzhnits, D. A., & Linde, A. D. 1976, Ann. Phys. (NY), 101, 195
Kolb, E. W., & Turner, M. S. 1990, The Early Universe (Reading: Addison-Wesley)
Kurki-Suonio, H. 1988, Phys. Rev. D, 37, 2104
Kurki-Suonio, H., Matzner, R. A., Centrella, J., Rothman, T., & Wilson, J. R. 1988, Phys. Rev. D, 38, 1091
Malaney, R. A., & Butler, M. N. 1989, Phys. Rev. Lett., 62, 117
Malaney, R. A., & Mathews, G. J. 1993, Phys. Rep., 229, 145
Mathews, G. J., Meyer, B. S., Alcock, C. R., & Fuller, G. M. 1990, ApJ, 358, 36
McLerran, L. 1989, Phys. Rev. Lett., 62, 1075
McLerran, L., Shaposhnikov, M., Turok, N., & Voloshin, M. 1991, Phys. Lett. B, 256, 451
Misner, C. W. 1967, Nature, 214, 40
Mueller, B. 1985, The Physics of the Quark-Gluon Plasma (Berlin: Springer-Verlag)
Nelson, A. 1990, Phys. Lett. B, 240, 179
Peebles, P. J. E. 1965, ApJ, 142, 1317
———. 1971, Physical Cosmology (Princeton: Princeton Univ. Press)
Petersson, B. 1991, Nucl. Phys. A, 525, 237c
Shaposhnikov, M. E. 1986, JETP Lett., 44, 465
———. 1987, Nucl. Phys. B, 287, 757
———. 1988, Nucl. Phys. B, 299, 797
Terasawa, N., & Sato, K. 1989a, Prog. Theor. Phys., 81, 254
———. 1989b, Phys. Rev. D, 39, 2893
———. 1989c, Prog. Theor. Phys., 81, 1085
———. 1990, ApJ, 362, L47
Turok, N., & Zadrozny, P. 1990, Phys. Rev. Lett., 65, 2331
———. 1991, Nucl. Phys. B, 358, 471
Wagoner, R. V., Fowler, W. A., & Hoyle, F. 1967, ApJ, 148, 3
Witten, E. 1984, Phys. Rev. D, 30, 272
Yokoyama, J., & Suto, Y. 1991, ApJ, 379, 427